Effect of initial density, particle shape and confining stress on the critical state behavior of weathered gap-graded granular soils

By

Xiusong Shi

Professor, Key Lab of Ministry of Education for Geomechanics and Embankment Engineering, Hohai University, Nanjing, China

Email: xiusongshi@hhu.edu.cn; qingsongsaint@gmail.com

Kai Liu (Corresponding author)

Doctoral student, Department of Civil and Environmental Engineering,

The Hong Kong Polytechnic University, Hung Hom, Kowloon, Hong Kong, China

Email: kevin-kai.liu@connect.polyu.hk

Jianhua Yin

Professor, Department of Civil and Environmental Engineering,

The Hong Kong Polytechnic University, Hung Hom, Kowloon, Hong Kong, China

Email: cejhyin@polyu.edu.hk

May 2020

Abstract

Weathered gap-graded soils are a common geological body in mountainous regions, and they are widely used as construction materials. The shear strength is controlling parameter for design of civil projects, however, there is still a controversy on the coarse fraction effect on the shear strength of gap-graded soils. To this end, 22 triaxial shear tests are performed on gap-graded soils, and the factors affecting the coarse fraction effect have been analyzed, including the confining stress, the particle shape of aggregates and the initial density of sand matrix. Partial contacts and sand bridges between aggregates are responsible for the transmission of loading and thus affect the coarse fraction effect. The results of triaxial tests reveal that: (1) The overall shear strength of sand-beads mixtures is rather independent of the confining stress and the coarse fraction, even the volume of aggregates is as high as 44.5%. (2) The effect of shape of aggregates is effective only at a high coarse volume fraction (44.5%) for loose-sand-gravel mixtures, where the partial contacts between aggregates plays an important role in forming the inter-aggregate structure. (3) The overall shear strength of gap-graded soils with denser matrix increases continuously with rising coarse fraction. The formation of densified sand bridge is correlated with the initial density of sand matrix, which contributes to the loading transmission in inter-aggregate structure, in turn, affects the overall critical state behavior of gap-graded soils. The insights drawn from this study provides a reference for assessing the deformation behavior of weathered residual soils.

Keywords: Shear strength; Critical State; Gap-graded soils; Coarse fraction; Mixture theory

Introduction

Gap-graded soils are usually induced by degradation of sandstones due to weathering factors in semi-arid areas. For example, sandstones usually contain clay minerals which are sensitive to dry-wetting cycles. This leads to a breakage of contacts between grains, and the sandstones disintegrate into separated particles due to seasonal moist changes; Consequently, the disintegrated particles fill the inter-aggregates voids, producing a mixture of coarse gravels and fine particles (Chandler, 2000; Xiao et al., 2016; Zhou et al., 2016; Qin and Chian, 2017; Park and Santamarina, 2017). The gap-graded granular soils can be also induced by transportation of residual soils, e.g., debris-flow deposits and proluvial deposits (Jiang et al., 2016; Peng et al., 2018; Cui et al., 2019; Tan et al., 2019; Guo and Cui, 2020). The structure of weathered gap-graded mixtures is analogous to that of other binary mixtures, such as fibre-reinforced composites (Nguyen and Fatahi, 2016; Kang and Bate, 2016; Fu and Coop, 2017; Chenari et al., 2018; Kang et al., 2018; Xiao et al., 2019a) which are widely used in pavement design and other civil engineering projects.

The structure and morphological features of gap-graded soils vary with their sources and the formation process (Xu et al., 2019c; Shi and Zhao, 2020). The weathered gap-graded soils are characterized into two types (Ruggeri et al., 2016): one with aggregate-sustained structure when the inter-aggregate skeleton prevails, and the other with matrix-sustained configuration when discrete aggregates floats in the fine matrix. “matrix-sustained” structure prevails in intensely weathered areas since the fine fraction is usually beyond the “transitional fine content” (Deng et al., 2017; Chen et al., 2019a; Shi et al., 2020). As a common geological body in mountainous regions, they are widely used as construction materials in engineering practices, including foundations, airports, embankments, and dams (Ruggeri et al., 2016; Zhou et al., 2017; Chen et al., 2019b). The stability of these infrastructures depends on the shear strength of gap-graded soils. The presence of coarse aggregates affects the shear

strength of residual soils. Hence, a better understanding of coarse fraction effect on the critical state behavior of gap-graded soils is critical for the stability analysis of geostructures.

Study on the shear behavior of gap-graded soils has been documented by many researchers. However, there is still controversy on the coarse effect on the shear strength of gap-graded soils. Some of them reported that the shear strength is approximately constant with the increase of coarse content up to a threshold (Xu et al., 2019a; Muir Wood and Kumar, 2000; Vallejo and Mawby, 2000). Other researchers concluded that the shear strength increases continuously with the coarse fraction (Yin, 1999; Jafari and Shafiee, 2004; Elkady et al., 2015; Ruggeri *et al*., 2016). The controversy may arise from a wide range of factors, including both the nature of aggregates and the fraction of phases, e.g., the particle size distribution, and particle shape of aggregates, the fraction and initial state of fine matrix, and the confining pressures (Yagiz, 2001; Shin and Santamarina, 2012; Elkady et al., 2015; Ruggeri et al., 2016; Zhao et al., 2018; Xiao et al., 2019b). For a better understanding of the above factors on the shear behavior of gap-graded soils, 22 triaxial compression tests are done on three types of gap-graded soils, including different coarse fractions, different particle shape and various initial void ratio of the fine matrix. The highlights of our work are as follow: (1) gap-graded soils with a prescribed void ratio of matrix are tested, so that the coarse fraction effect are separated and assessed; (2) the effect of initial state of matrix are evaluated, which is seldom reported by previous researchers; (3) the critical state behavior of gap-graded soils is discussed, and the mechanisms governing the coarse fraction effect are addressed.

Materials and approach

Gap-graded materials

Gap-graded soils rich in fine sand particles occur extensively in mountainous areas in western

China (Chen et al., 2019a; Xu et al., 2019b). An example of this type of materials is a weathered residual soil (from Chongqing province, China) with a deficiency of particle size between 0.425 mm and 2.0 mm. The particle size distribution curve indicates a coefficient of uniformity of 35.47. The fine particles in gap-graded soil originate from the disintegration of intact sandstones due to weathering process, and the coarse gravels is strongly weathered due to moist change. The weathered aggregates may collapse during preparation, saturation, consolidation and shearing process. To avoid the disintegration of aggregates and focus on the effect of coarse fraction, the coarse aggregates are replaced by steel beads and feldspar gravels. Previous work on random particulate composites suggests that the overall stiffness is controlled by fine matrix after the stiffness of inclusions surpasses a certain value (Tu *et al.*, 2005). Therefore, the difference in stiffness of aggregates may not lead to a distinct difference in the overall behavior. Fig. 1 shows the fines, steels beads, gravels and their mixtures. The steel beads are spherical and most of the gravel particles have a subangular shape.

The basic physical properties of the aggregates are given in Table 1. The diameter of coarse particles varies between 2.0 mm and 20 mm, and the particle size distribution (both steel beads and gravels) is consistent with that of the gravels in the weathered residual soil. The specific gravity of the steel beads and the gravel is 7.90 Mg/m^3 and 2.65 Mg/m^3, respectively. The fine particles of the residual soil smaller than 0.425 mm is used as the fines for the mixtures. It has a maximum void ratio of 1.323 and a minimum void ratio of 0.406. The maximum dry density of the fines is 1.94 Mg/m^3, and the optimum moisture content is 12%. The density of fine soil particles is 2.73 Mg/m^3. The particle size distribution of fines is given in Table 1. It is seen that the fine matrix has a negligible fraction of clay particles (diameter<0.002 mm).

Fines are mixed with different amounts of steel beads or gravel to obtain various gap-graded mixtures. Details of the soil specimens and triaxial tests are given in Table 2. Five

initial volume fractions of the coarse particles are adopted, designated as 0%, 9.9%~10.0%, 20.0%, 32.2%~32.3%, and 44.5%, respectively. Note that the coarse fraction denotes the dry mass fraction of coarse aggregates in the sequel, unless otherwise specified. A maximum volume fraction of 44.5% is adopted for the coarse aggregates, since this study is on the matrix-sustained structure of gap-graded soils. The results of this work may provide a reference for the strong weathered soils or of core of embankment dams, where the fines are dominant in gap-graded soils.

The main purpose of this study is to investigate the coarse fraction effect of the shear behavior of gap-graded soils. To this end, three series of triaxial tests are done: (1) Series-1, loose sand matrix mixed with steel beads. Five different coarse fractions (by mass, from 0% to 79.7%) and three different confining stress (200 kPa, 300 kPa and 450 kPa) are considered in this series. (2) Series-2, loose sand matrix mixed with feldspar gravels. All the tests are done at a confining stress of 300 kPa, and five different coarse fractions (by mass) are considered, varying from 0% to 56.9%. and (3) Series-3, dense sand matrix mixed with gravel. The tests are done at 300 kPa, with coarse fraction (by mass) from 0% to 55.0%. Correspondingly, three factors affecting the coarse fraction effect are investigated in this study: (1) The effect of confining stress can be clarified based on the results of Series-1. (2) Since the particle shape is distinctly different between the steel beads and feldspar gravels, the effect of particle shape of aggregates is highlighted by comparing Series-1 with Series-2; (3) The same coarse aggregates are adopted in Series-2 and Series-3, hence, one distinguishes the effect of the initial density of fine matrix.

Sample preparation

The initial size of triaxial specimens is 10 cm in diameter and 20 cm in height. All the specimens were prepared using a moist tamping technique. First, water was added to the fines for an initial water content of 12%, and it was kept inside a plastic bag for several hours for a

moisture homogenization. Then, the fines were mixed with the coarse material (steel beads or gravel) in room conditions. Afterward, the sample was compacted inside a cylindrical mold in 5 layers (using a vibrating hammer). The top surface of each layer was scored for a better bonding between adjacent layers. Finally, the specimen was extruded from the mold to triaxial cell for saturation, consolidation and compression process. Note that the type of coarse aggregates and initial density of fine matrix are the same in each series of triaxial tests. In this case, the effect of coarse fraction can be evaluated. The particles size distribution curves of the gap-graded samples are shown in Fig. 2, including different type of aggregates, various initial densities and coarse fractions. The particle size distribution curve of sand-steel beads mixtures lies below the one containing gravel due to the high density of steel beads. For the gap-graded soils, the gravels float in sand matrix. It prevents breakage of the aggregates during the triaxial loading process. Therefore, the particle size distribution of gravels remains unchanged.

Test procedures

The compacted specimen was extruded from the cylindrical mold to the triaxial cell and sealed with a membrane. Afterward, a small effective confining stress was applied to hold the specimen. Two methods are adopted for saturation of the specimens: First, carbon dioxide (CO_2) was percolated through the specimens for more than 10 hours, followed by a flooding of deaired water from the bottom of the specimens. Further, the specimen was saturated by applying a back pressure of at least 200 kPa. Following the two procedures, the B value of Skempton's pore water pressure parameter is higher than 0.97. Finally, the effective confining stress was increase to a desired consolidation stress. Table 2 summarizes the testing program for the specimens. After being fully consolidated, drained triaxial tests were done under a constant loading rate of 0.1mm/min. The triaxial tests were stopped if the asymptotic state is approached or the axial strain is higher than 20%. The axial deformation, axial load, and

174 volume change of the specimens were recorded during the loading process.

175

176 **Variables of gap-graded soils**

177 The gap-graded soils in this study are a mixture of sand and coarse aggregates (steel beads or
178 gravels). In this kind of mixture system, the two phases possess distinctly different stiffness
179 (Weng, 1990; Tu et al., 2005; Shi and Yin, 2018; Shi et al., 2019), and the deformation can be
180 assumed to be fully concentrated within the sand matrix. As reported by previous researchers,
181 the volume average approach can well describe the behavior of gap-graded mixtures (Tandon
182 and Weng, 1988; Shi et al., 2020). If the strain variables are defined as volume-average values,
183 one derives the relationship between the overall strains and the values of matrix

184 $$\varepsilon_p = (1-\phi_a)\varepsilon_{ps};\ \varepsilon_q = (1-\phi_a)\varepsilon_{qs} \tag{1}$$

185 where ε_{ps} and ε_{qs} are volumetric strain and deviatoric strain of the sand matrix, respectively;
186 ε_p and ε_q are the corresponding overall strains of the gap-graded soils; ϕ_a is the volume
187 fraction of the coarse aggregates, which is equivalent to the inter-aggregate void ratio adopted
188 by others (Thevanayagam and Mohan, 2000, Monkul and Ozden, 2007; Deng et al., 2017).
189 Obviously, the volume fraction varies during the loading process, and ϕ_a is a function of the
190 overall void ratio e and the void ratio of sand matrix e_s (Shi et al., 2020). Considering that
191 the aggregates are incompressible, the overall void ratio and sand void ratio are correlated,
192 and one calculates the volume fraction of aggregates. Note that two types of fractions are used:
193 the dry mass fraction ψ_a and the volume fraction ϕ_a of aggregates. The dry mass fraction is
194 constant during mechanical process in laboratory testing. However, in constitutive modeling
195 and numerical simulations, the volume fraction ϕ_a varies with stress level, therefore, it is
196 usually used for homogenizing state variables of inhomogeneous soils, e.g., Eq. (1).

The incremental stress in the matrix usually differs from that of in the aggregates during loading process (de Boer, 2006; Shi and Yin, 2018). However, the stress in the constituents is difficult to be measured for the cohesionless soils due to the initial density effect (Chandler, 2000). Therefore, only the overall stresses in the gap-graded soils are analyzed in this work. Two overall stress invariants, p' (overall effective mean stress) and q (deviatoric stress), are adopted. Both are defined as the volume average values.

Test results of gap-graded soils

The overall behavior of particle-reinforced gap-graded soils relies on both the soil matrix and the inter-aggregate structure. As previously mentioned, three factors may contribute to the coarse fraction effect of gap-graded soils: the confining stress, the particle shape of aggregates, and the initial density of sand matrix. In the sequel, these factors will be analyzed based on the test results. In order to highlight the mentioned factors, the initial void ratio of the sand matrix in gap-graded specimens are the same for each series of tests.

Behavior of pure sands

It is well recognized that the behavior of matrix is a frame of reference for assessing the effect of particle-reinforced soil mixtures (Tandon and Weng, 1988; Shi et al., 2020). A series of conventional drained triaxial tests were performed on the pure sands at different confining pressures (Table 2). Two different initial densities are adopted, with relative densities of 0.69 and 0.82, respectively. Fig. 3 presents two diagrams with the test results for the pure sands, including the evolution of stress ratio and volumetric strain. It is seen that both the dense and loose specimens show a strain-hardening behavior during triaxial loading. The stiffness of denser one is higher than that of the loose one, and the volumetric deformation of the denser specimens is much lower than that of the loose ones. However, the asymptotic state of them is

221 approximately the same.

222 The Critical State Line of the pure sand is shown in Fig. 4, both on the stress plane and the
223 compression plane. Corresponding to the limit stress ratio in Fig. 3, the critical state of sand
224 specimens (both loose and denser ones) in p'-q stress plane can be well approximated by a
225 unique line though the origin:

226 $$q_s = M_s p'_s \tag{2}$$

227 where M_s=1.29 is a strength parameter. As the overall stresses are the equivalent to the values
228 of matrix in pure sands, the subscript "s" is used in Eq. (2) to distinguish between the pure
229 sand matrix and gap-graded specimens. The critical state points of the pure sand in
230 compression plane are shown in Fig. 4b in semi-logarithmic plot. The critical state of sand for
231 different initial densities shows almost a unique relationship. The void ratio of sand decreases
232 nonlinearly with the effective mean stress, which is consistent with the data for cohesionless
233 soils from literature (e.g., Verdugo and Ishihara,1996; Riemer and Seed 1997; Sun et al.,
234 2019). To this end, the empirical equation proposed by Li and Wang (1998) are adopted for
235 the Critical State Line of pure sand:

236 $$e_s = e_{\Gamma s} - \lambda_s \left(\frac{p'_s}{p_a} \right)^{\xi} \tag{3}$$

237 where $e_{\Gamma s}$, λ_s and ξ are parameters of the critical state formula, the subscript "s" denotes pure
238 sand material. There are three model parameters in Eq. (3), where $e_{\Gamma s}$ corresponds to the void
239 ratio at an infinitely value of small stress, λ_s is the slope of the compression line in terms of
240 $e_s \sim \left(p'_s / p_a \right)^{\xi}$ relationship, and ξ represents the curvature of the curves in $e_s \sim p'_s / p_a$
241 relationship. As noted by Li and Wang (1998), the value of ξ varies between 0.6 and 0.8.
242 ξ=0.6 is adopted in this work, and the other two parameters can be easily calibrated ($e_{\Gamma s}$
243 =0.561, and λ_s =0.043). In practical applications, one may simply choose a default value of ξ

for developing the expressions of the critical state lines of interest.

Effect of confining stress

The test results may be not reliable enough in case of small stress levels. Therefore, we choose a minimum effective confining stress of 200 kPa. According to the previous study on the weathered residual soils, the sand particles in fine matrix may collapse at high stress levels. In this case, the particle degradation of fine sand particles is involved, and coarse fraction effect cannot be qualitatively assessed. Therefore, the effective confining stress between 200 kPa-450 kPa is adopted. For investigating of the effect of confining stress, the initial density of sand matrix (e_s=0.695) is prescribed for all the specimens in this series. A loose matrix is adopted in this work to avoid the effect of over-consolidation on the shear behavior. It is assumed that the coarse aggregates and the sand matrix are "fully mixed". 'fully mixed' denotes that the aggregates float homogeneously in the matrix when the sand fraction is higher than the inter-aggregate porosity. The initial void ratios of the gap-graded specimens are listed in Table. 2, which decreases with the coarse fraction (by dry mass).

Results of drained triaxial shear tests on gap-graded soils with different fractions of coarse steel beads, from 0% to 79.7%, are shown in Figure 5. The result of gap-graded soils is more pronounced at higher confining stress levels (300 kPa in Fig. 5b and 450 kPa in Fig. 5c). The initial shear stiffness increases as the coarse fraction increases; however, the peak value of overall stress ratio appears to be rather independent of the coarse fraction, even the coarse fraction approaches 79.7%. This is consistent with the published results that the stress ratio of the gap-graded soils is controlled by the mechanical behavior of the fine matrix for a matrix sustained structure (Xu et al., 2019b). The initial stiffness of gap-graded soils at lower stress level (200 kPa) is approximately the same at low coarse fractions (below 55.1%), which is probably due to the initial compaction during preparation process.

Change of overall volumetric strain with overall deviatoric strain are shown in Fig. 6. In

contrast with the stress ratio, the volumetric strain at various confining stress levels is significantly affected by coarse fraction. As the steel beads are incompressible compared with the softer sand matrix, the asymptotic volumetric strain falls as the coarse fraction increases. Thanks to the incompressible aggregates, the strain variables of sand matrix are calculated by Eq. (1). The change of overall stress ratio and volumetric strain of sand matrix (denoted as "sand volumetric strain") with the deviatoric strain of sand matrix (denoted as "sand deviatoric strain") are shown in Fig. 7a and Fig. 7b, respectively. It is found that both the overall stress ratio and the sand volumetric strain are essentially independent of coarse fraction, even the fraction of steel beads reaches 79.7%.

The critical state points of the gap-graded soils with various coarse fractions are plotted in Fig. 8a, together with the Critical State Line of pure sand. It indicates that the critical state of gap-graded soils (steel beads as inclusions) is well consistent with the Critical State Line of pure sands, regardless of confining stress and coarse fractions. The critical state points of the gap-graded soils on compression plane are summarized in Fig. 8b. The solid and dotted lines are Critical State Lines of gap-graded soils following Li and Wang (1998):

$$e = e_{\Gamma} - \lambda \left(\frac{p'}{p_a} \right)^{\xi} \tag{4}$$

Note that e_{Γ} and λ are the critical state parameters for gap-graded soils, different from the parameters $e_{\Gamma s}$ and λ_s in Eq. (3). The values of calibrated model parameters are given in Table 3. Both e_{Γ} and λ falls as the coarse fraction increases, since the presence of aggregates reduces the compressibility of the gap-graded soils.

Effect of particle shape of aggregates

In the first series of tests, gap-graded soils with a high fraction of steel beads (79.7%) is tested at a confining stress of 300 kPa, with an initial coarse volume fraction as high as 44.5% (Fig

292 5b). The initial stiffness is significantly higher than that of the pure sand. However, after
293 approaching its maximum value (overall deviatoric strain of 12%), the mixture shows a strain-
294 softening behavior. As a result, the critical state shear strength is slightly lower than that of
295 the pure sand. This differs from the results of sand-kaolin mixtures (Muir Wood and Kumar,
296 2000). In their study, the limit stress ratio is significantly higher than that of the pure clay
297 matrix at a volume fraction of 45% (sand aggregates). The inconsistency between the
298 previous work and this study may be induced by the shape of coarse aggregates. To this end,
299 the effect of particle shape of aggregates is evaluated by replacing the steel beads with
300 granular gravels.

301 To highlight the effect of particle shape of aggregates, the initial void ratio of sand matrix
302 (loose matrix, e_s=0.695) and the initial volume fraction of aggregates are designated. Both are
303 the same as the first series (Table 2). Fig. 9 summarizes the results of drained triaxial tests on
304 sand-gravel mixtures at an effective confining stress of 300 kPa. Analogous to the first series,
305 the initial stiffness rises as the coarse fraction increases. The asymptotic stress ratio appears to
306 be unchanged as the coarse fraction increases from 0% to 43.9%. However, it shows a striking
307 increase at a coarse fraction of 56.9%, with an initial volume fraction of 44.5%. The overall
308 volumetric strain reduces with increasing coarse fraction, and the results are comparable to
309 those of the sand-steel beads mixtures.

310 The change of overall stress ratio and sand volumetric strain are plotted in Fig. 10, it is found
311 once again that both the overall stiffness and volumetric deformation of sand matrix are
312 independent of coarse fraction until the coarse fraction reaches 56.9%. The critical state points
313 are plotted in Fig. 11. The ultimate stress ratio is in good agreement with the Critical State
314 Line of pure sand as the coarse fraction increases from 0% to 43.9%. However, the ultimate
315 stress ratio deviates from the Critical State line at a coarse fraction of 56.9%. Obviously, this
316 conclusion is not consistent with the results in the first series, and this difference arises from

317 the different particle shape of coarse aggregates in these two series of tests. As shown in Fig.
318 11b, the critical state points of sand-gravel mixtures are approximately close to the
319 corresponding Critical State Lines of sand-steel beads mixtures.

320 *Effect of initial density of sand matrix*

321 The effect of initial density of clay slurry on the compression behavior of sand-clay mixtures
322 is done by Shi and Yin (2017) and Shi et al. (2018). However, the effect initial density of
323 fines on shear behavior of gap-graded soils is seldomly reported by previous researchers. To
324 reveal the influence of matrix density on the coarse fraction effect of gap-graded soils, the
325 third series of triaxial tests (dense matrix, e_s=0.570) are done in comparison with the second
326 series (loose matrix, e_s=0.695). The granular feldspar gravels, as adopted in the second series,
327 are used for creating the mixtures.
328 The relationship between overall stress ratio (volumetric strain) and overall deviatoric strain
329 for the gap-graded soils with various coarse fractions (third series) is shown in Fig. 12. It is
330 seen that the curves show strain-hardening and volume-contraction behavior for all specimens.
331 In general, both the stiffness and ultimate shear strength increases continuously with rising
332 coarse aggregates, as the coarse fraction increases from 0% to 55.5%. This is consistent with
333 the results of various compacted gap-graded soils from literature (e.g., Yin, 1999; Jafari and
334 Shafiee, 2004; Ruggeri et al., 2016; Xu et al., 2019b). The change of overall stress ratio and
335 sand volumetric strain with sand deviatoric strain is shown in Fig. 13. The volume change of
336 sand matrix is analogous to the first series and second series, which is independent with the
337 coarse fraction. The effect of coarse fraction on stiffness vanishes within small strain ranges,
338 and the curves with various coarse fraction deviate as the sand deviatoric strain increases.
339 This reveals that the deviatoric stress becomes more nonuniform with the shearing process.
340 As illustrated in Fig. 14a, the critical state points of gap-graded soils in stress plane deviates
341 from the Critical State Line of pure sand as the coarse fraction increases. However, the critical

state points in the compression plane are located approximately on the corresponding Critical State Lines of the gap-graded soils containing steel beads (Fig. 14b). This is due to different effect of structure change on the effective mean stress p' and deviator stress q: the effective mean stress in gap-graded soils is more uniform than the deviator stress.

The difference in compression curves of gap-graded soils (Figs 11 and 14) originates from the coarse fraction. With increase of coarse fraction, the deformable sand matrix is replaced by solid aggregates. Therefore, the compression curve moves downwards as the coarse fraction rises. The curves with different coarse fractions tend to be converged, since the deformable fine sand matrix is densified with increasing stress level. However, the curves tend to converge toward zero, i.e., the fine sand matrix becomes a solid, at extremely high stress level.

Discussions

The strongly weathered residual soils usually possess a matrix-sustained structure, and the overall behavior is mainly controlled by the sand matrix, but still partially affected by the presence of coarse aggregates. The above section presents the present three factors affecting the coarse fraction effect of gap-graded soils. The mechanisms governing their influence on coarse fraction are tentatively discussed in the sequel.

Two phenomena may be responsible for the transmission of inter-aggregate forces and thus affect the reinforcement of coarse inclusions: (1) partial contacts between aggregates, and (2) sand bridges within gap-graded soils (Fig. 15). The partial contacts between the aggregates arises from the nonuniform distribution of coarse inclusions (Shi et al., 2019). The number of contacts rises with the increasing coarse fraction. The sand bridges form due to the densification of sand matrix between adjacent coarse aggregates. This stiff sand layer acts like a bridge, which contributes to the loading transmission in inter-aggregate structure (Jafari and

Shafiee 2004; Shi et al., 2019).

The effect of initial void ratio on the mechanical behavior of gap-graded soils can be classified into two points: (1) the volume fraction of aggregates decreases as the initial void ratio increases. This leads to a decreasing number of contacts between aggregates, and the coarse fraction effect becomes weaker. (2) The loading bearing capacity of densified sand bridges becomes lower with the increase of initial void ratio; therefore, the sand bridge is more fragile, which collapses easily during shear process. For the gap-graded soils mixed with loose sand matrix and steel beads, the two phases are fully mixed during the comparation process, therefore, the number of partial contact is smaller, and the reinforcement of coarse aggregates is negligible. The overall mechanical response is controlled entirely by the sand matrix up to a coarse volume fraction of 44.5%. For the gap-graded soils mixed with loose sand matrix and granular gravels, the inter-aggregate structure is weak at low coarse fractions (below 43.9%), but the increasing partial contacts start to transmit the force and reinforce the inter-aggregate structure at a volume fraction (coarse) of 44.5%. Therefore, the stiffness and shear strength are higher than those of the pure matrix, as well as the sand-steel beads mixture with coarse fraction of 79.7% (volume fraction = 44.5%). For the gap-graded soils mixed with dense sand and steel beads, the sand bridge forms during compaction and consolidation. The densified sand bridge may contribute to the continuous increase of shear strength with coarse fraction. At a volume fraction of 44.5% (coarse), the striking increase of shear strength is attributed to the combining effect of the partial contacts and sand bridge between coarse aggregates.

The method described by Clayton et al. (2009) is adopted to quantify two average two-dimensional shape parameters of aggregates, including aspect ratio and roundness. A similar method used by Altuhafi et al. (2016) is adopted to study this effect. After the image acquisition and analysis, average values of aspect ratio and roundness of aggregates are

calculated based on the particle size distribution of coarse aggregates (Fig. 1c). The values are summarized in Table 2. Note that the values of shape parameters are based on digital image processing (DIP) method (Chen et al., 2020). The methods used in 3D type usually use Xray μCT and 3D laser scanner, which is more realistic. In general, the aspect ratio from 2D analysis is smaller than the 3D values due to the preferred orientation of minor axes (Chen et al., 2020).

There are extensive previous work on clay-sand or clay-gravel mixtures (e.g., Yin, 1999; Jafari and Shafiee, 2004; Monkul and Ozden, 2007; Elkady et al., 2017; Deng et al., 2017; Shi and Yin, 2017; Shi et al., 2018), and the evolution of its structure is investigated. However, the matrix of sand-gravel mixtures in this study is different from the mixtures with cohesive matrix. This leads to significant mechanical behavior between the two soils, e.g., its state-dependent behavior. The normal compression line of clays is usually supposed to be unique, however the compression behavior of granular soils strongly depends on its initial state (Elkady et al., 2015; Shi and Yin, 2017; Bian et al., 2020; Shi and Zhao, 2020). This would have distinct influence on the overall mechanical behavior of gap-graded soils.

Conclusions

Three series of triaxial shear tests has been done on gap-graded soils to investigate the coarse fraction effect, and to analyze the factors affecting the coarse fraction effect, including the confining stress, the particle shape and the initial density of sand matrix. Conclusions are summarized as follows:

(1) The shear strength of sand-beads mixtures is independent of both the confining stress and the coarse fraction, even the coarse volume fraction reaches as high as 44.5%. This is due to fragile sand bridge and negligible number of partial contacts between aggregates.

(2) The shear strength of loose sand-gravel mixtures is independent of the coarse fraction at

low volume fraction of aggregates. The effect of particle shape of aggregates is effective only at a high coarse fraction of 44.5%, where the partial contacts between aggregates plays an important role in forming the inter-aggregate structure.

(3) The shear strength of dense sand-gravel mixtures increases continuously with rising coarse aggregates, as the coarse volume fraction increases from 0% to 44.5%. This is due to the densified sand bridge between the aggregates, which in turn, affects the overall behavior of gap-graded soils.

Data Availability Statement

Some or all data, models, or code that support the findings of this study are available from the corresponding author upon reasonable request. (data in Figs 2-14).

Acknowledgments

This study was partially supported by the National Natural Science Foundation of China (under Grant No. 51908193). The work in this paper is also supported by the Fundamental Research Funds for the Central Universities (under Grant no. B200201050), three RGC/GRF projects (Grant No. 16201419; PolyU 152196/14E; PolyU 152796/16E), a CRF project (Grant No.: PolyU12/CRF/13E) from Research Grants Council (RGC) of Hong Kong Special Administrative Region Government (HKSARG) of China. The authors also acknowledge the financial supports from Research Institute for Sustainable Urban Development of The Hong Kong Polytechnic University, grants (1-ZVCR, 1-ZVEH, 4-BCAU, 4-BCAW, 5-ZDAF, G-YN97) from The Hong Kong Polytechnic University.

References

Altuhafi, F. N., Coop, M. R., & Georgiannou, V. N. (2016). Effect of particle shape on the mechanical behavior of natural sands. *Journal of Geotechnical and Geoenvironmental Engineering*, 142(12), 04016071.

Bian, X., Cui, Y. J., Zeng, L. L., & Li, X. Z. (2020). State of compacted bentonite inside a fractured granite cylinder after infiltration. *Applied Clay Science*, 186, 105438.

Chandler, R. J. (2000). The Third Glossop Lecture: Clay sediments in depositional basins: the geotechnical cycle. *Quarterly Journal of Engineering Geology and Hydrogeology*, 33(1), 7-39.

Chen W. B., Borana L., Feng W. Q., Yin J. H. & Liu K. (2019a). Influence of matric suction on nonlinear time-dependent compression behaviour of a granular fill material. *Acta Geotechnica*, 13, 1-19.

Chen, W. B., Liu, K., Yin, Z. Y., & Yin, J. H. (2020). Crushing and flooding effects on one-dimensional time-dependent behaviors of a granular soil. *International Journal of Geomechanics*, 20(2), 04019156.

Chen, W. B., Yin, J. H., & Feng, W. Q. (2019b). A new double-cell system for measuring volume change of a soil specimen under monotonic or cyclic loading. *Acta Geotechnica*, 14(1), 71-81.

Chenari, R. J., Fatahi, B., Ghorbani, A., & Alamoti, M. N. (2018). Evaluation of strength properties of cement stabilized sand mixed with EPS beads and fly ash. *Geomechanics and Engineering*, 14(6), 533-544.

Clayton, C. R. I., Abbireddy, C. O. R., & Schiebel, R. (2009). A method of estimating the form of coarse particulates. *Géotechnique*, 59(6), 493-501.

Cui, Y. F., Jiang, Y., & Guo, C. X. (2019). Investigation of the initiation of shallow failure in widely graded loose soil slopes considering interstitial flow and surface runoff. *Landslides*,

16(4), 815-828.

De Boer, R. (2006). Trends in continuum mechanics of porous media (Vol. 18). *Springer Science & Business Media*.

Deng, Y., Wu, Z., Cui, Y., Liu, S., & Wang, Q. (2017). Sand fraction effect on hydro-mechanical behavior of sand-clay mixture. *Applied Clay Science*, 135, 355-361.

Elkady, T. Y., Shaker, A. A., & Dhowain, A. W. (2015). Shear strengths and volume changes of sand-attapulgite clay mixtures. *Bulletin of Engineering Geology and the Environment*, 74(2), 595-609.

Fu, R., Coop, M. R., & Li, X. Q. (2017). Influence of particle type on the mechanics of sand-rubber mixtures. *Journal of Geotechnical and Geoenvironmental Engineering*, 143(9), 04017059.

Gomez, J. S., Chalaturnyk, R. J., & Zambrano-Narvaez, G. (2019). Experimental investigation of the mechanical behavior and permeability of 3D printed sandstone analogues under triaxial conditions. *Transport in Porous Media*, 129(2), 541-557.

Guo, C. X., Cui, Y. F. (2020) Pore structure characteristics of debris flow source material in the Wenchuan earthquake area. *Engineering Geology*, 267, 105499

Jafari, M. K., & Shafiee, A. (2004). Mechanical behavior of compacted composite clays. *Canadian Geotechnical Journal*, 41(6), 1152-1167.

Jiang, N. J., Soga, K., & Kuo, M. (2016). Microbially induced carbonate precipitation for seepage-induced internal erosion control in sand-clay mixtures. *Journal of Geotechnical and Geoenvironmental Engineering*, 143(3), 04016100.

Kang, X., & Bate, B. (2016). Shear wave velocity and its anisotropy of organically modified high volume class fly ash-kaolinite mixtures, *Journal of Geotechnical and Geoenvironmental Engineering*, ASCE, 143, 04016068.

Kang, X., Cao, J., & Bate, B. (2018). Large-strain strength of polymer-modified kaolinite and

fly ash-kaolinite mixtures. *Journal of Geotechnical and Geoenvironmental Engineering*, 145(2), 04018106.

Li, X. S., & Wang, Y. (1998). Linear representation of steady-state line for sand. *Journal of Geotechnical and Geoenvironmental Engineering*, 124(12), 1215-1217.

Monkul, M. M., & Ozden, G. (2007). Compressional behavior of clayey sand and transition fines content. *Engineering Geology*, 89(3), 195-205.

Muir Wood, D., & Kumar, G. V. (2000). Experimental observations of behaviour of heterogeneous soils. *Mechanics of Cohesive-frictional Materials: An International Journal on Experiments, Modelling and Computation of Materials and Structures*, 5(5), 373-398.

Nguyen, L., & Fatahi, B. (2016). Behaviour of clay treated with cement & fibre while capturing cementation degradation and fibre failure-C3F Model. I*nternational Journal of Plasticity*, 81, 168-195.

Park, J., & Santamarina, J. C. (2017). Revised soil classification system for coarse-fine mixtures. *Journal of Geotechnical and Geoenvironmental Engineering*, 143(8), 04017039.

Peng, D., Xu, Q., Liu, F., He, Y., Zhang, S., Qi, X., ... & Zhang, X. (2018). Distribution and failure modes of the landslides in Heitai terrace, China. *Engineering Geology*, 236, 97-110.

Qin, C. B., & Chian, S. C. (2017). Kinematic analysis of seismic slope stability with a discretisation technique and pseudo-dynamic approach: a new perspective. *Géotechnique*, 68(6), 492-503.

Riemer, M. F., & Seed, R. B. (1997). Factors affecting apparent position of steady-state line. *Journal of Geotechnical and Geoenvironmental Engineering*, 123(3), 281-288.

Ruggeri, P., Segato, D., Fruzzetti, V. M. E., & Scarpelli, G. (2016). Evaluating the shear strength of a natural heterogeneous soil using reconstituted mixtures. *Géotechnique*, 66(11), 941-946.

Shi, X. S., Nie, J., Zhao, J., & Gao, Y. (2020). A homogenization equation for the small strain

517 stiffness of gap-graded granular materials. *Computers and Geotechnics*, 121, 103440.
518 Shi, X. S., & Yin, J. (2017). Experimental and theoretical investigation on the compression
519 behavior of sand-marine clay mixtures within homogenization framework. *Computers and*
520 *Geotechnics*, 90, 14-26.
521 Shi, X. S., & Yin, J. (2018). Consolidation behavior for saturated sand-marine clay mixtures
522 considering the intergranular structure evolution. *Journal of Engineering Mechanics*,
523 144(2), 04017166.
524 Shi, X. S., & Zhao, J. (2020). Practical estimation of compression behavior of clayey/silty
525 sands using equivalent void-ratio concept. *Journal of Geotechnical and Geoenvironmental*
526 *Engineering*, 146(6), 04020046.
527 Shi, X. S., Zhao, J., Yin, J., & Yu, Z. (2019). An elastoplastic model for gap-graded soils
528 based on homogenization theory. *International Journal of Solids and Structures*. 163, 1-14.
529 Shin, H., & Santamarina, J. C. (2012). Role of particle angularity on the mechanical behavior
530 of granular mixtures. *Journal of Geotechnical and Geoenvironmental Engineering*, 139(2),
531 353-355.
532 Sun, Y., Gao, Y., & Zhu, Q. (2018). Fractional order plasticity modelling of state-dependent
533 behaviour of granular soils without using plastic potential. *International Journal of*
534 *Plasticity*, 102, 53-69.
535 Tan, D. Y., Yin, J. H., Feng, W. Q., Zhu, Z. H., Qin, J. Q., & Chen, W. B. (2019). New
536 Simple Method for Calculating impact force on flexible barrier considering partial muddy
537 debris flow passing through. *Journal of Geotechnical and Geoenvironmental Engineering*,
538 145(9), 04019051.
539 Tandon, G. P., & Weng, G. J. (1988). A theory of particle-reinforced plasticity. *Journal of*
540 *Applied Mechanics*, 55(1), 126-135.
541 Thevanayagam, S., & Mohan, S. (2000). Intergranular state variables and stress-strain

behaviour of silty sands. *Géotechnique*, 50(1), 1-23.

Tu, S. T., Cai, W. Z., Yin, Y., & Ling, X. (2005). Numerical simulation of saturation behavior of physical properties in composites with randomly distributed second-phase. *Journal of composite materials*, 39(7), 617-631.

Vallejo, L. E., & Mawby, R. (2000). Porosity influence on the shear strength of granular material-clay mixtures. *Engineering Geology*, 58(2), 125-136.

Verdugo, R., & Ishihara, K. (1996). The steady state of sandy soils. *Soils and foundations*, 36(2), 81-91.

Weng, G. J. (1990). The overall elastoplastic stress-strain relations of dual-phase metals. *Journal of the Mechanics and Physics of Solids*, 38(3), 419-441.

Xiao, Y., Coop, M. R., Liu, H., Liu, H., & Jiang, J. (2016). Transitional behaviors in well-graded coarse granular soils. *Journal of Geotechnical and Geoenvironmental Engineering*, 142(12), 06016018.

Xiao, Y., Nan, B., & McCartney, J. S. (2019a). Thermal conductivity of sand-tire shred mixtures. *Journal of Geotechnical and Geoenvironmental Engineering*, 145(11), 06019012.

Xiao, Y., Stuedlein, A. W., Ran, J., Evans, T. M., Cheng, L., Liu, H., ... & Chu, J. (2019b). effect of particle shape on strength and stiffness of biocemented glass beads. *Journal of Geotechnical and Geoenvironmental Engineering*, 145(11), 06019016.

Xu, D. S., Liu, H. B., Rui, R., & Gao, Y. (2019a). Cyclic and postcyclic simple shear behavior of binary sand-gravel mixtures with various gravel contents. *Soil Dynamics and Earthquake Engineering*, 123, 230-241.

Xu, D. S., Tang, J. Y., Zou, Y., Rui, R., & Liu, H. B. (2019b). Macro and micro investigation of gravel content on simple shear behavior of sand-gravel mixture. *Construction and Building Materials*, 221, 730-744.

Xu, D. S., Tang, Z., & Zhang, L. (2019c). Interpretation of coarse effect in simple shear

behavior of binary sand-gravel mixture by DEM with authentic particle shape. *Construction and Building Materials*, 195, 292-304.

Yagiz, S. (2001). Brief note on the influence of shape and percentage of gravel on the shear strength of sand and gravel mixtures. *Bulletin of Engineering Geology and the Environment*, 60(4), 321-323.

Yin, J. H. (1999). Properties and behavior of Hong Kong marine deposits with different clay contents. *Canadian Geotechnical Journal*, 36(6), 1085-1095.

Zhao, B., & Wang, J. (2016). 3D quantitative shape analysis on form, roundness, and compactness with μCT. *Powder technology*, 291, 262-275.

Zhao, S., Evans, T. M., & Zhou, X. (2018). Effects of curvature-related DEM contact model on the macro-and micro-mechanical behaviours of granular soils. *Géotechnique*, 17, 158.

Zhou, W. H., Xu, X., & Garg, A. (2016). Measurement of unsaturated shear strength parameters of silty sand and its correlation with unconfined compressive strength. *Measurement*, 93, 351-358.

List of tables

Table 1: Basic properties of the tested materials

Tested materials	Density of particles (Mg/m^3)	Clay (%)	Silt (%)	Sand (%)	Gravel (%)		
					2-5mm	5-10mm	10-20mm
Sand	2.73	1.8	9.6	88.6	0	0	0
Steel beads	7.90	0	0	0	27.5	32.7	39.8
Gravel	2.65	0	0	0	27.5	32.7	39.8

Table 2: Details of the soil specimens and triaxial tests

Soil type	Coarse fraction (%)		Effective consolidation stress (kPa)	Void ratio (After compaction)	Void ratio (After consolidation)	Aspect ratio (-)	Roundness (-)
	dry mass	volume					
Loose sand	0	0	200	0.695	0.562	-	-
	0	0	300	0.695	0.537		
	0	0	450	0.695	0.504		
Dense sand	0	0	300	0.570	0.503	-	-
Loose sand + steel beads	35.2	10.0	200	0.585	0.476	1.00	1.00
	35.2	10.0	300	0.585	0.456		
	35.2	10.0	450	0.585	0.431		
	55.1	20.0	200	0.488	0.404		
	55.1	20.0	300	0.488	0.387		
	55.1	20.0	450	0.488	0.365		
	70.0	32.2	200	0.385	0.312		
	70.0	32.2	300	0.385	0.300		
	70.0	32.2	450	0.385	0.286		
	79.7	44.5	300	0.294	0.250		
Loose sand + gravel	15.3	9.9	300	0.586	0.442	1.35	0.76
	29.1	20.0	300	0.488	0.370		
	43.9	32.3	300	0.385	0.304		
	56.9	44.5	300	0.294	0.236		
Dense sand + gravel	14.1	9.9	300	0.486	0.432	1.35	0.76
	27.6	20.0	300	0.409	0.364		
	42.0	32.3	300	0.326	0.287		
	55.0	44.5	300	0.252	0.225		

Table 3: Critical state parameters of the sand-steel beads mixtures

Coarse fraction (%)	0	35.2	55.1	70.0
e_Γ	0.561	0.480	0.406	0.289
λ	0.043	0.037	0.031	0.014

Figure 1a

Click here to access/download;Figure;Fig 1a.pdf

Figure 1b

Click here to access/download;Figure;Fig 1b.pdf

Figure 1c

Click here to access/download;Figure;Fig 1c.pdf

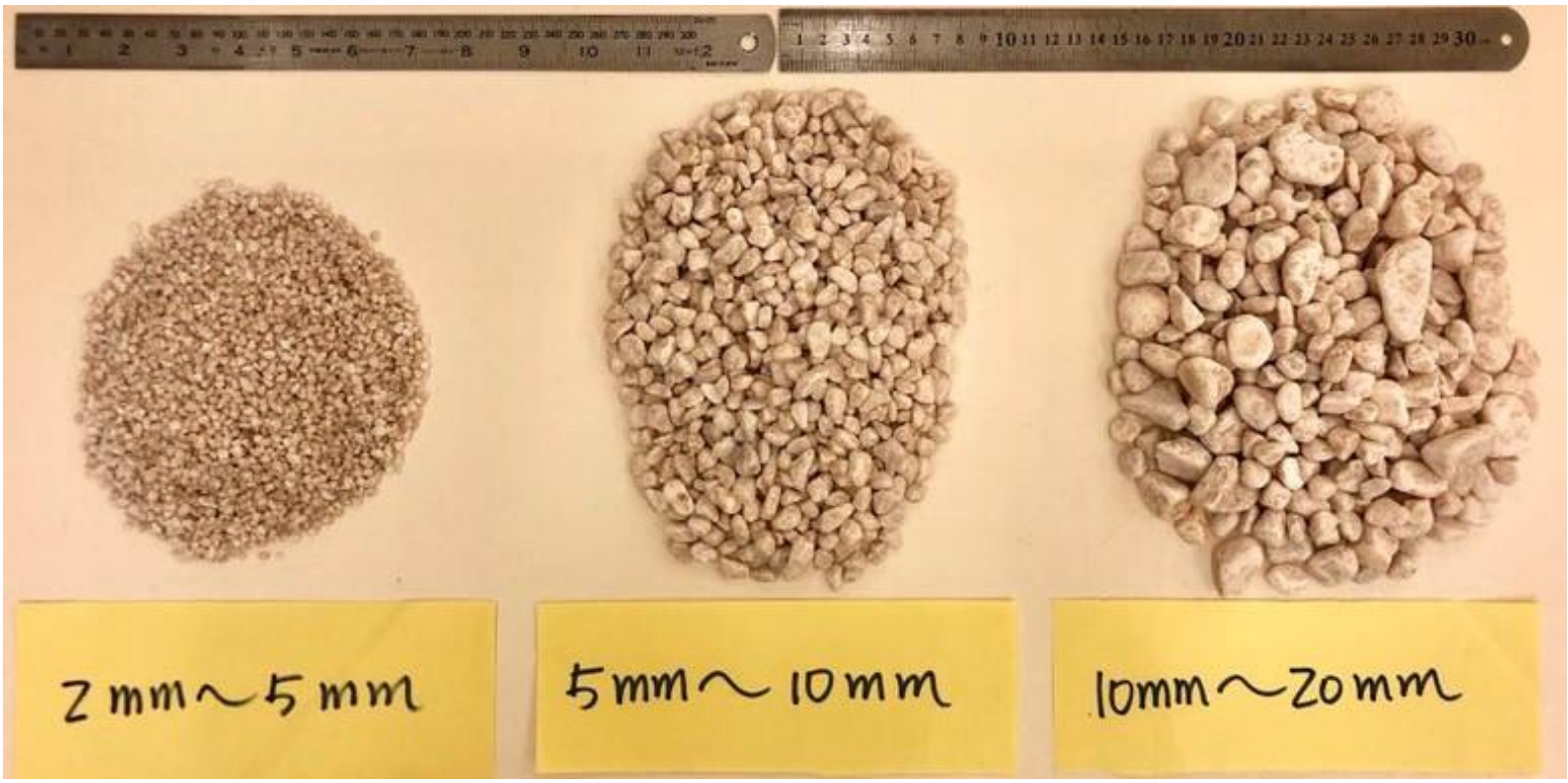

Figure 2a

Click here to access/download;Figure;Fig 2a.eps

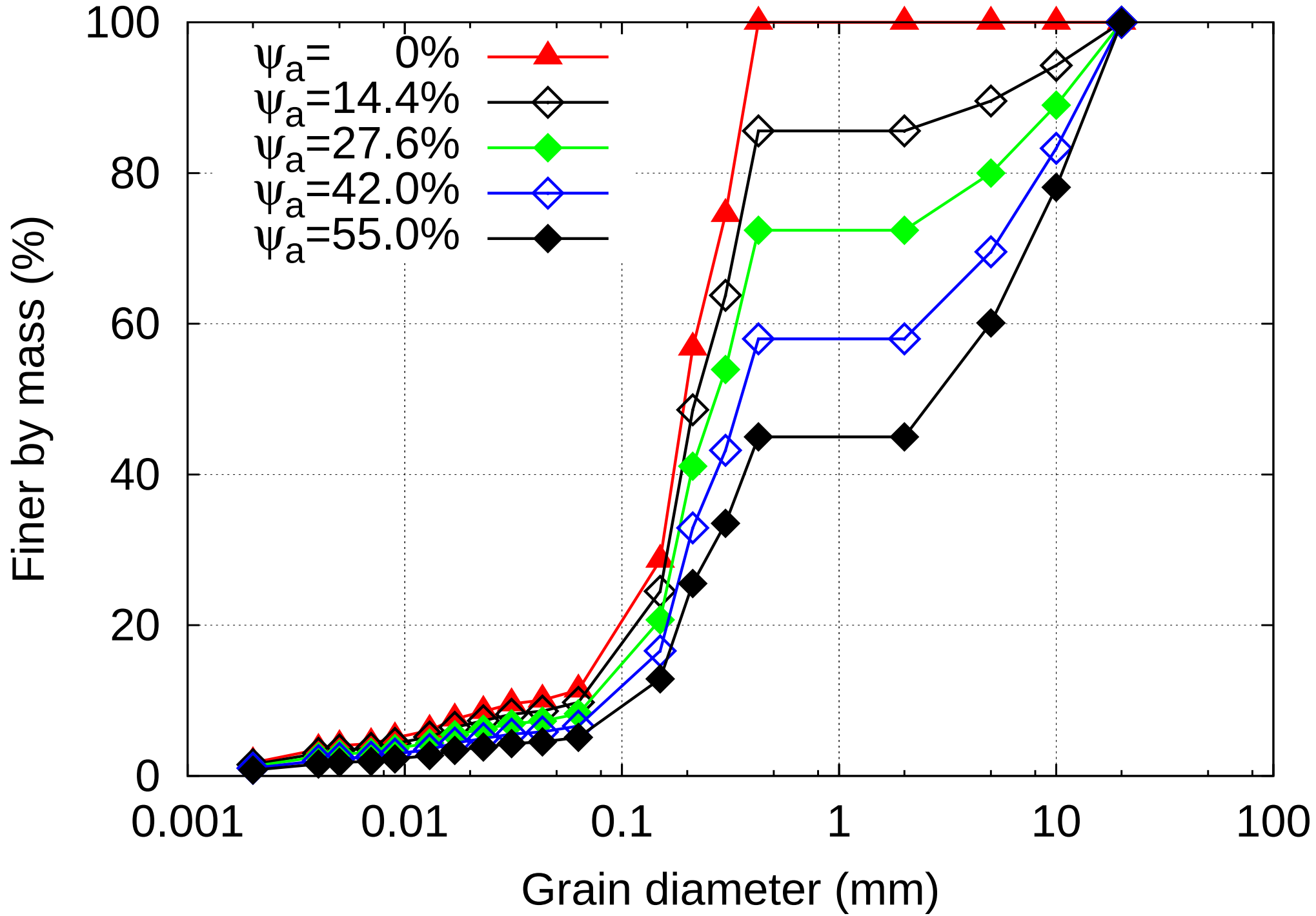

Figure 2b

Click here to access/download;Figure;Fig 2b.eps

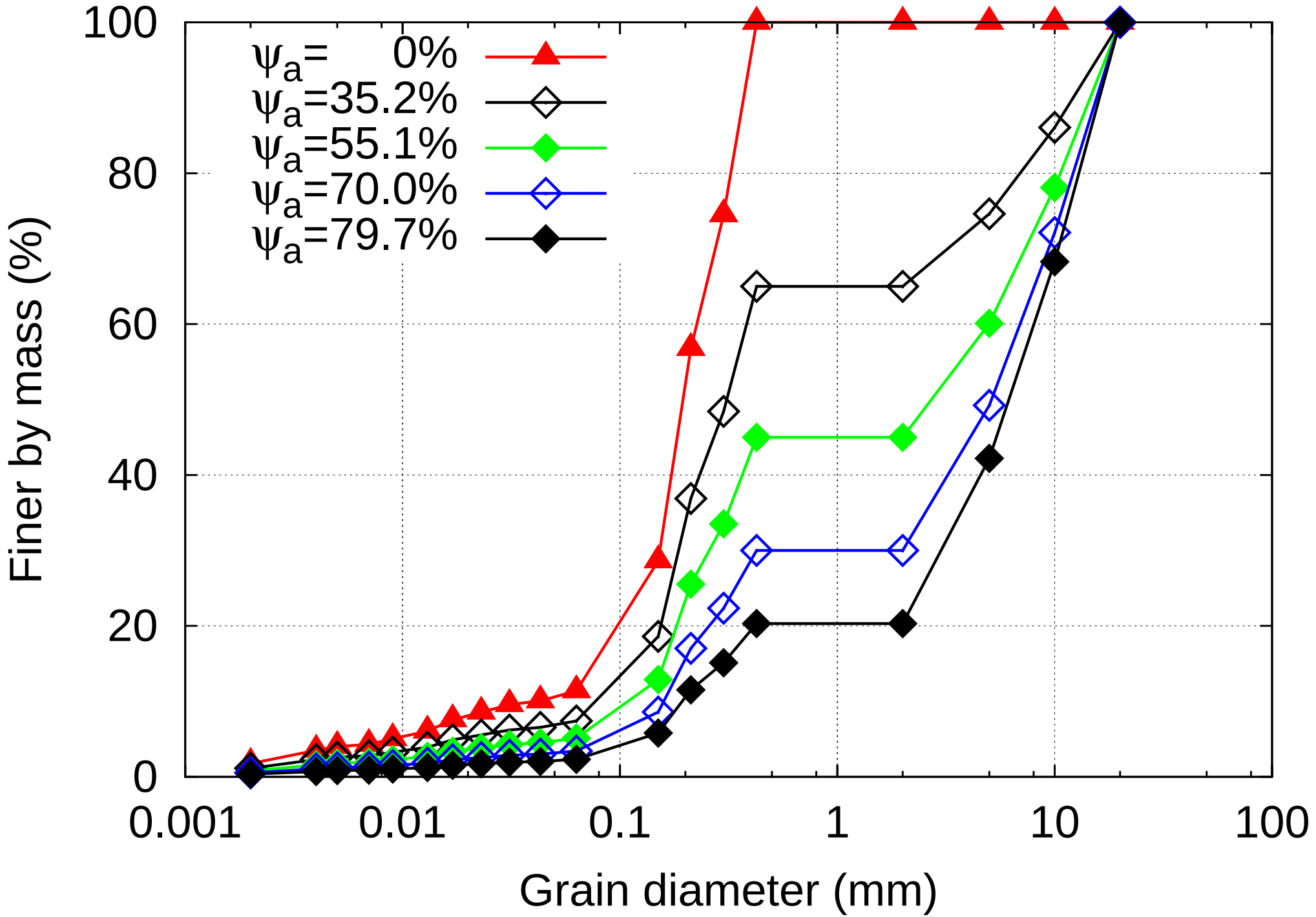

Figure 2c

Click here to access/download;Figure;Fig 2c.eps

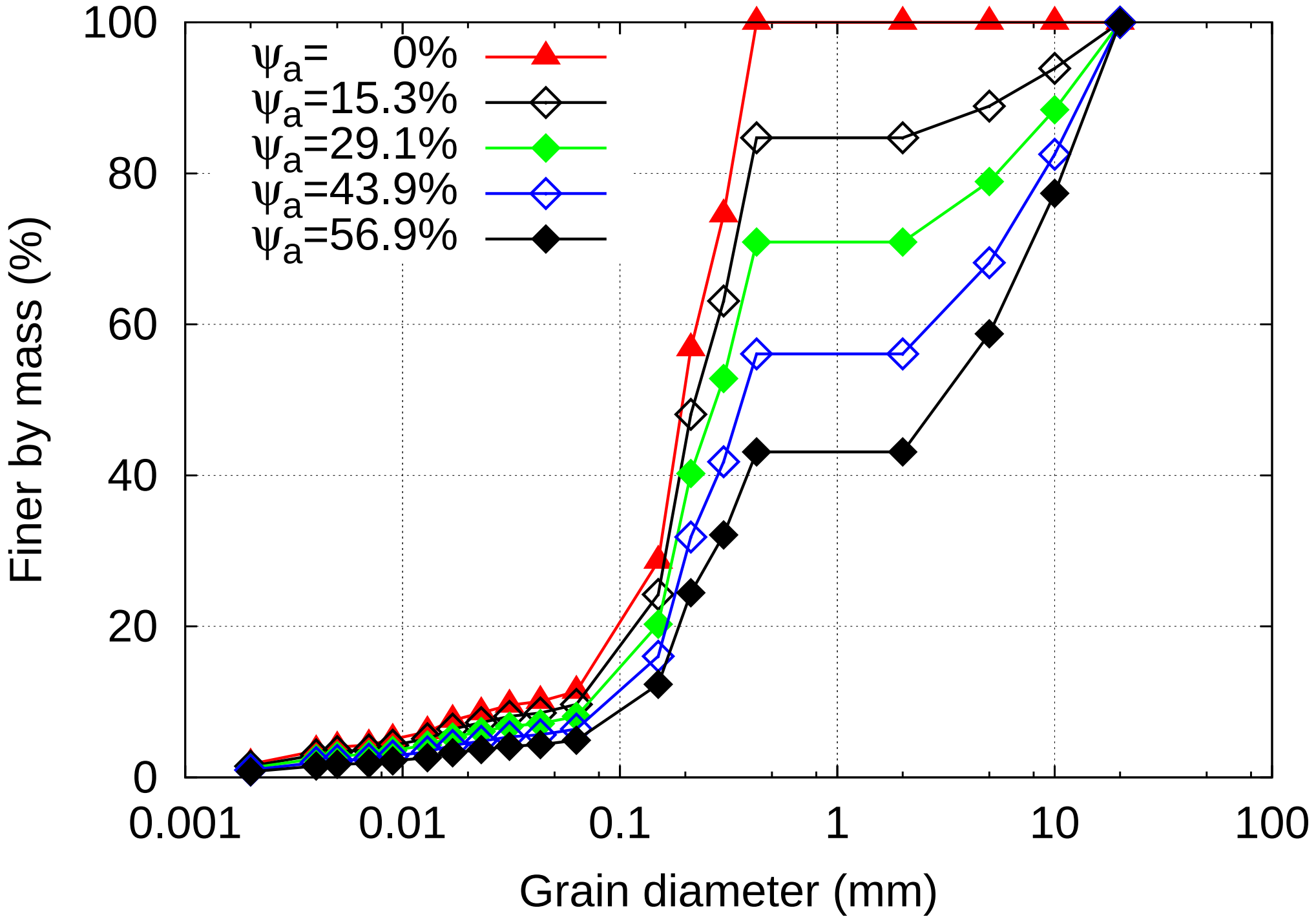

Figure 3a

Click here to access/download;Figure;Fig 3a.eps

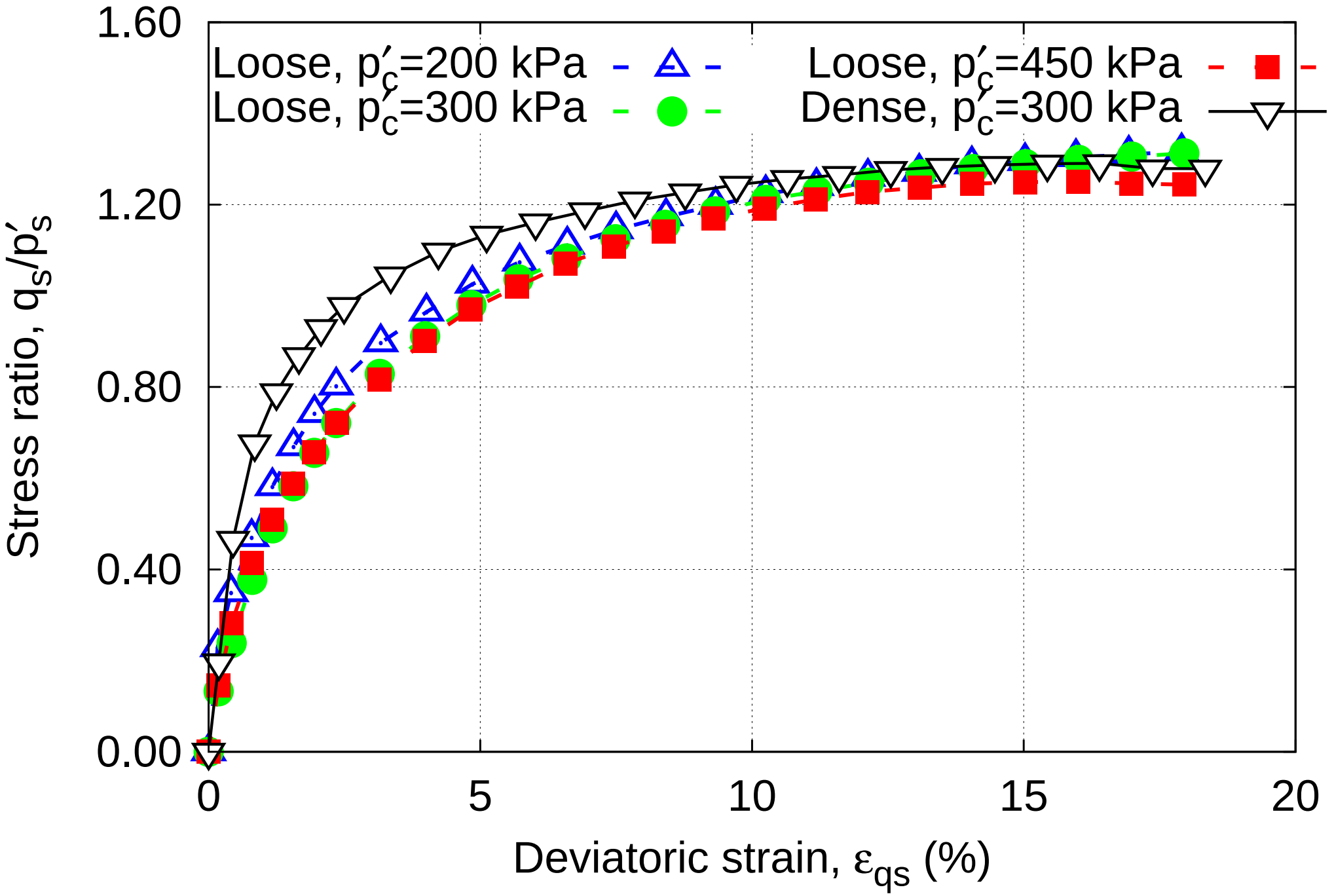

Figure 3b

Click here to access/download;Figure;Fig 3b.eps

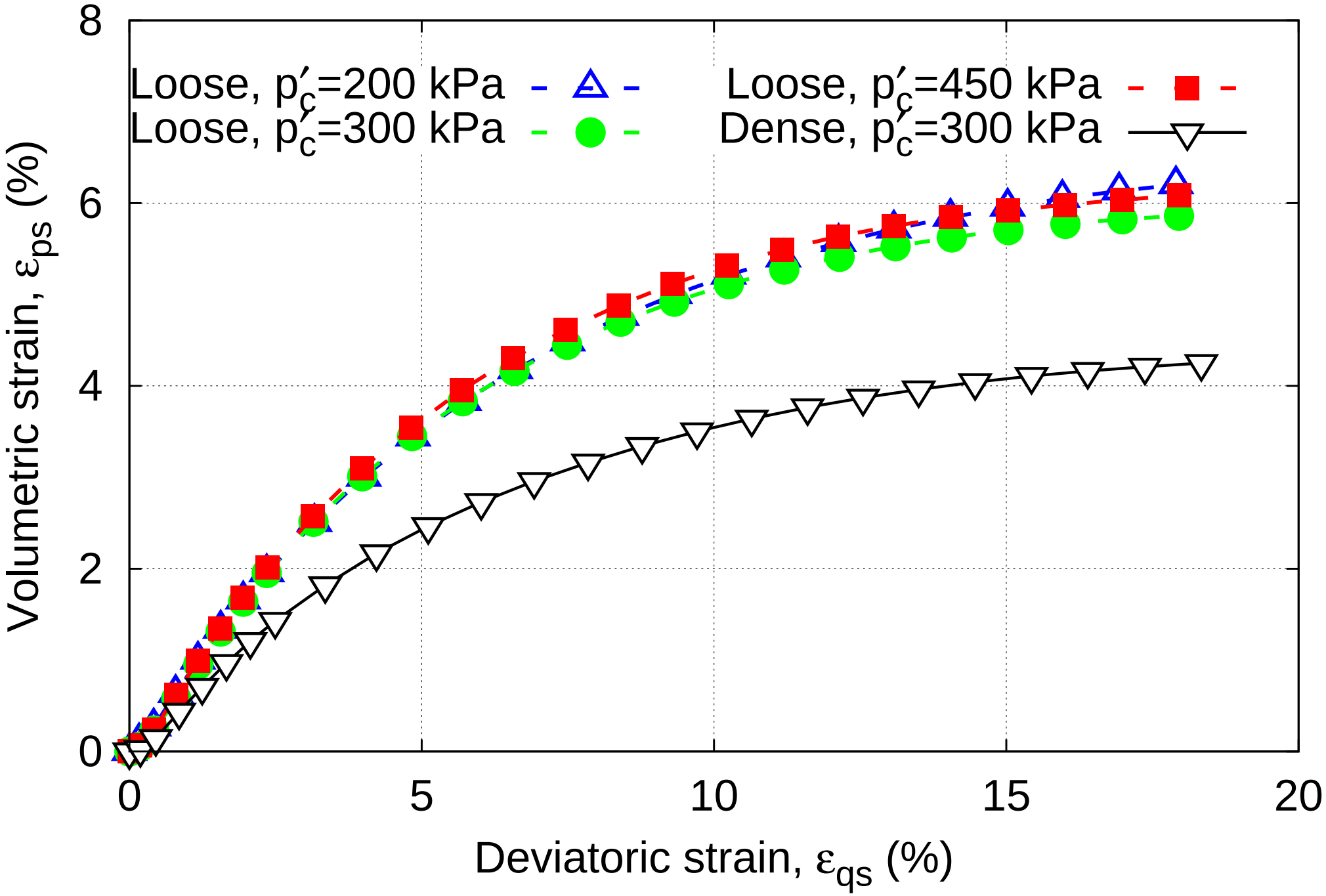

Figure 4a

Click here to access/download;Figure;Fig 4a.eps

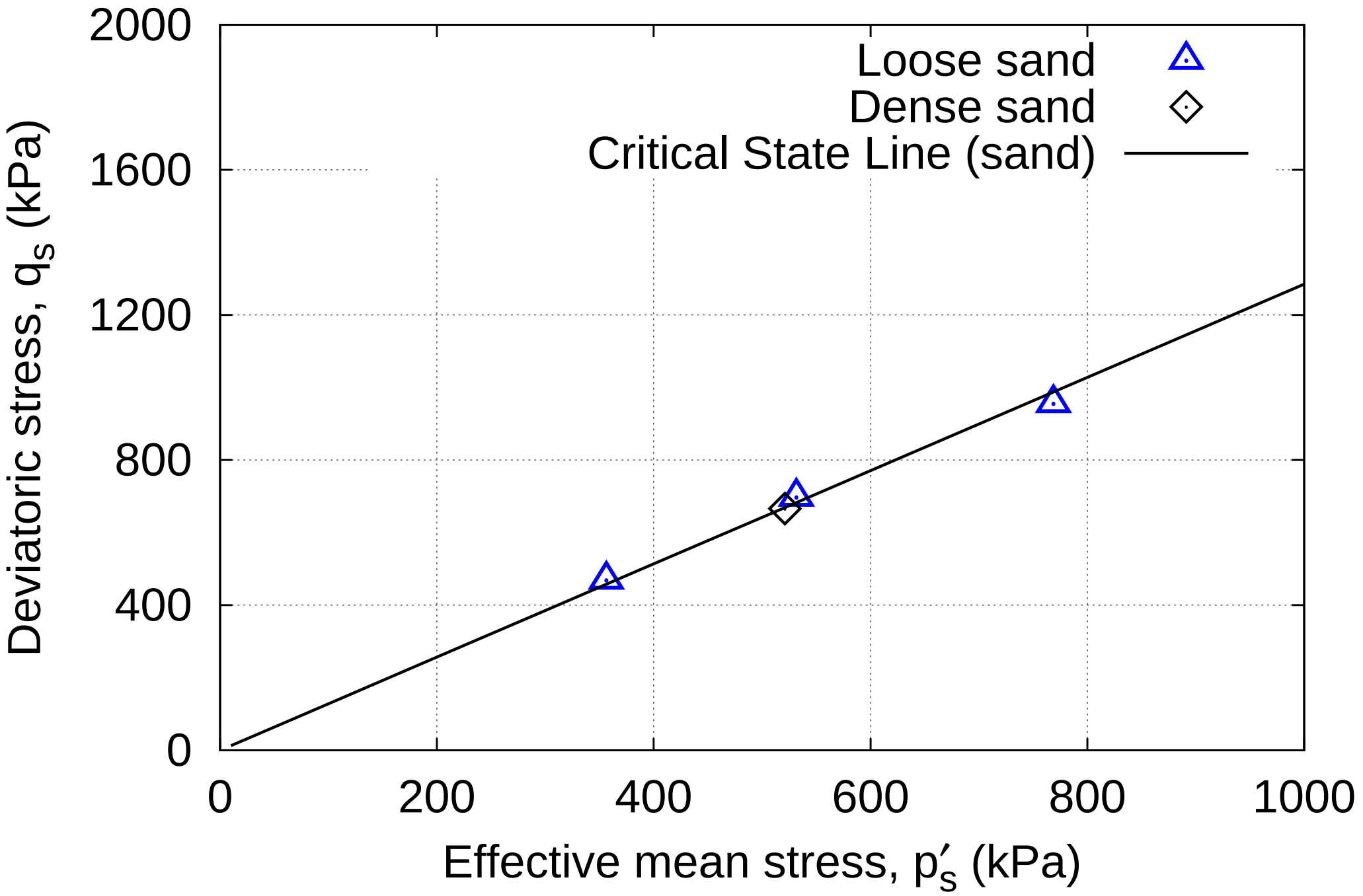

Figure 4b

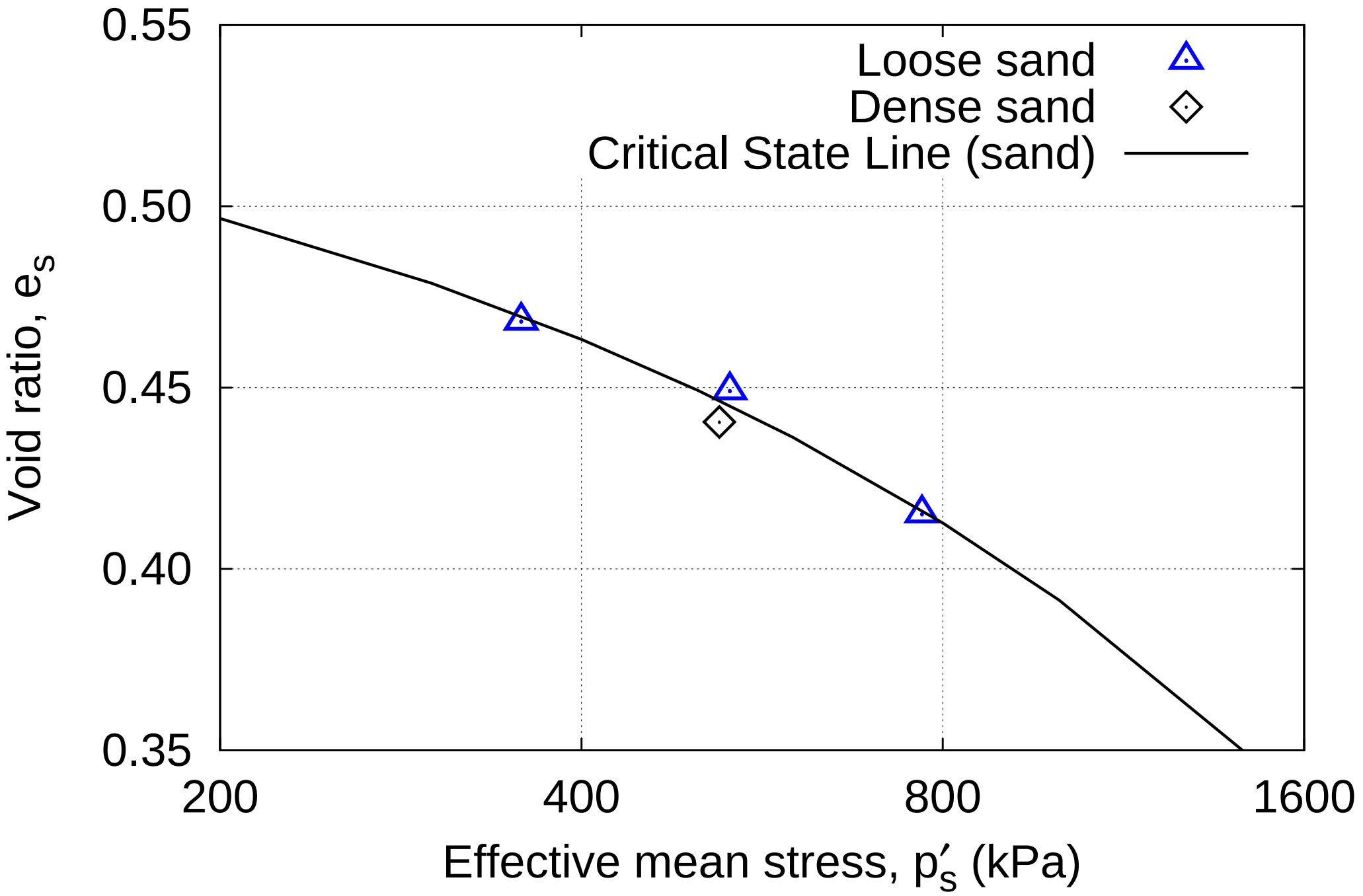

Figure 5a

Click here to access/download;Figure;Fig 5a.eps

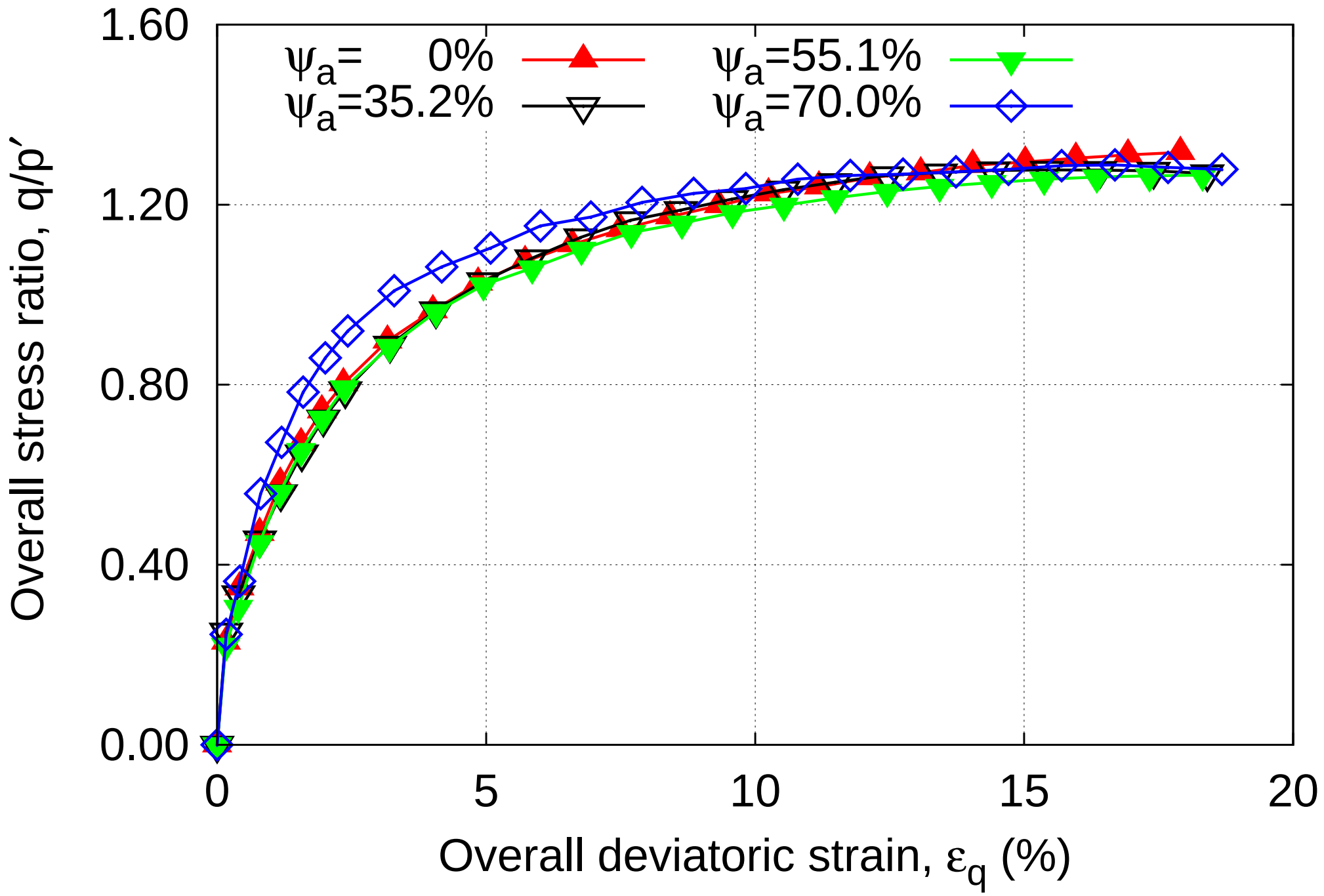

Figure 5b

Click here to access/download;Figure;Fig 5b.eps

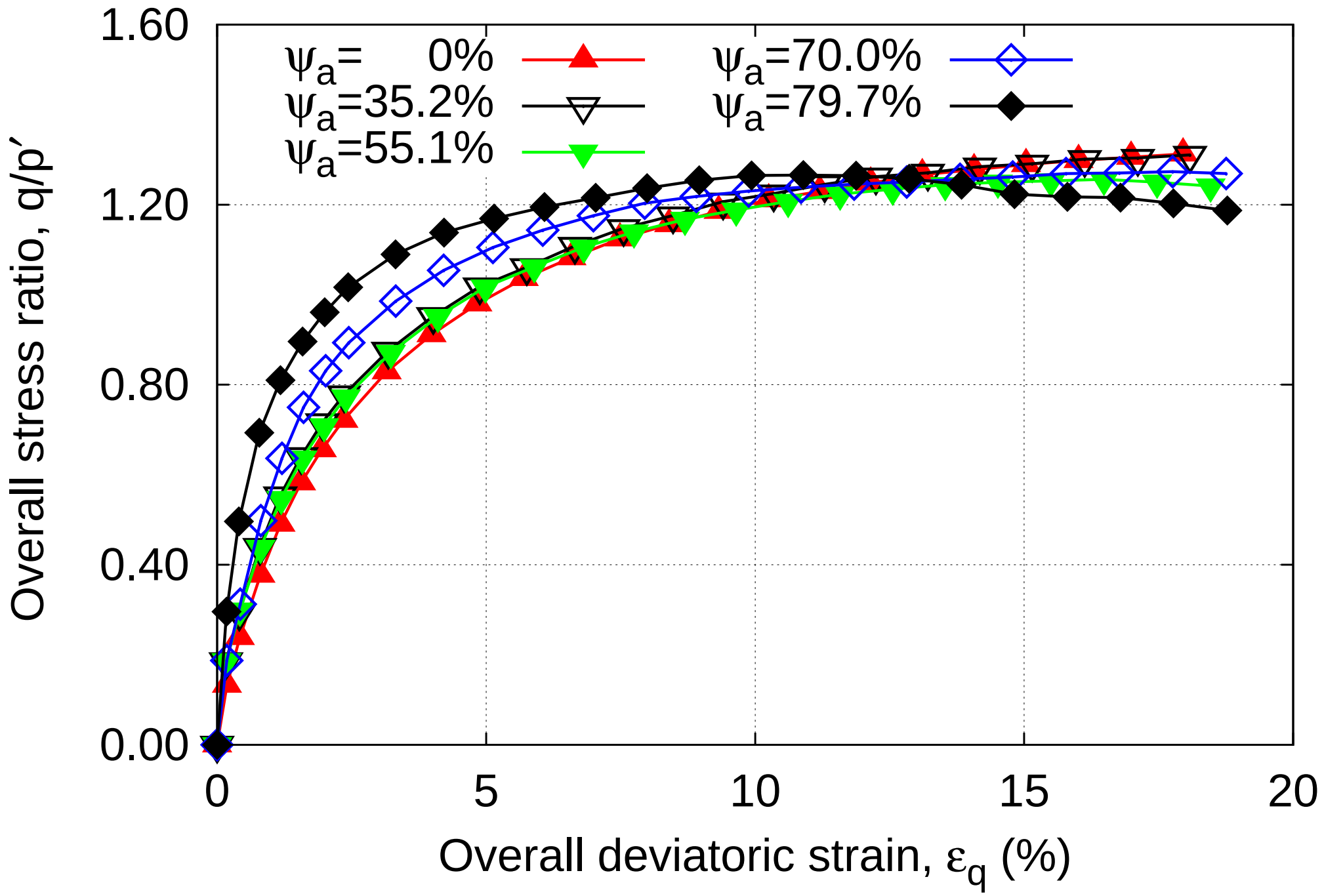

Figure 5c

Click here to access/download;Figure;Fig 5c.eps

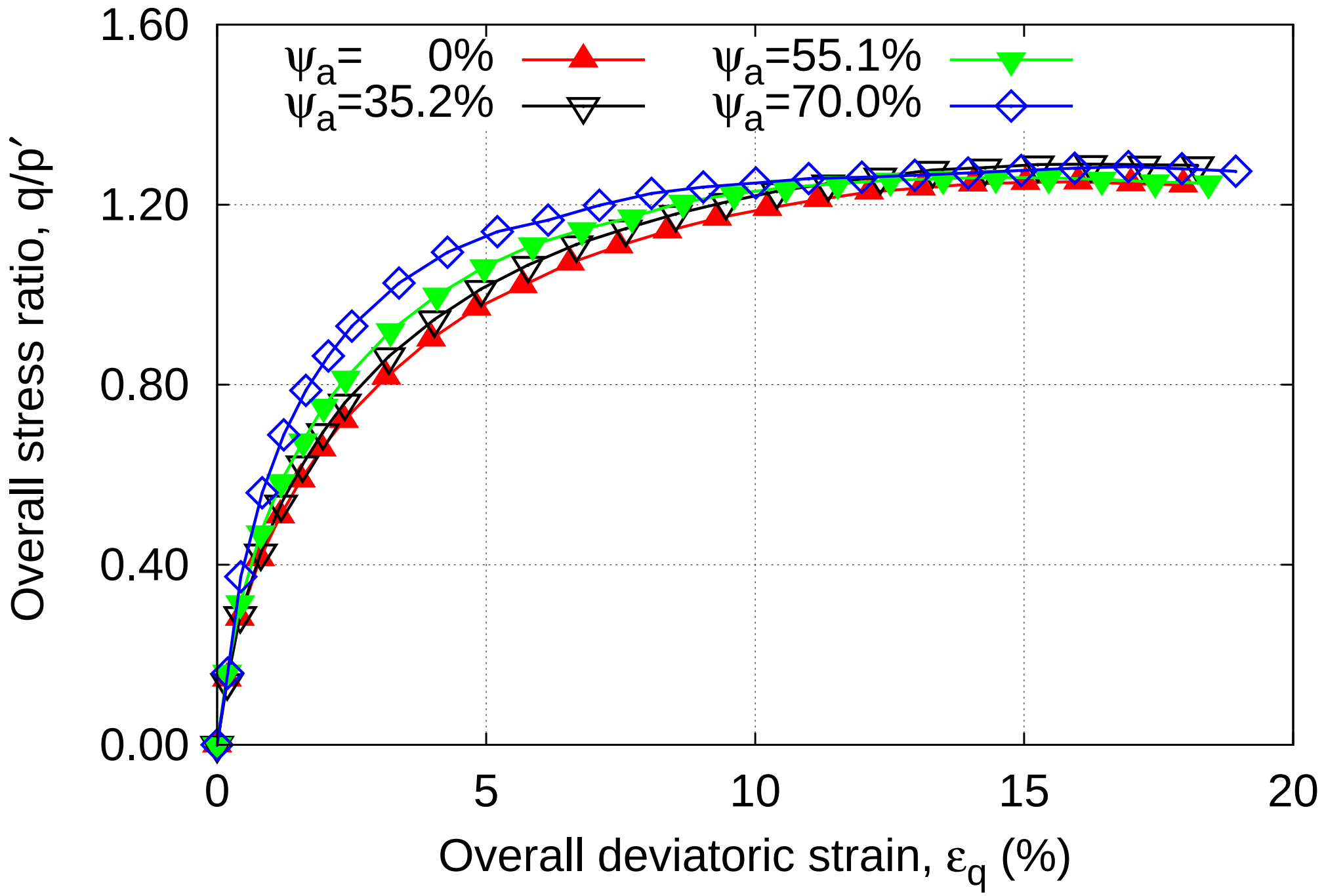

Figure 6a

Click here to access/download;Figure;Fig 6a.eps

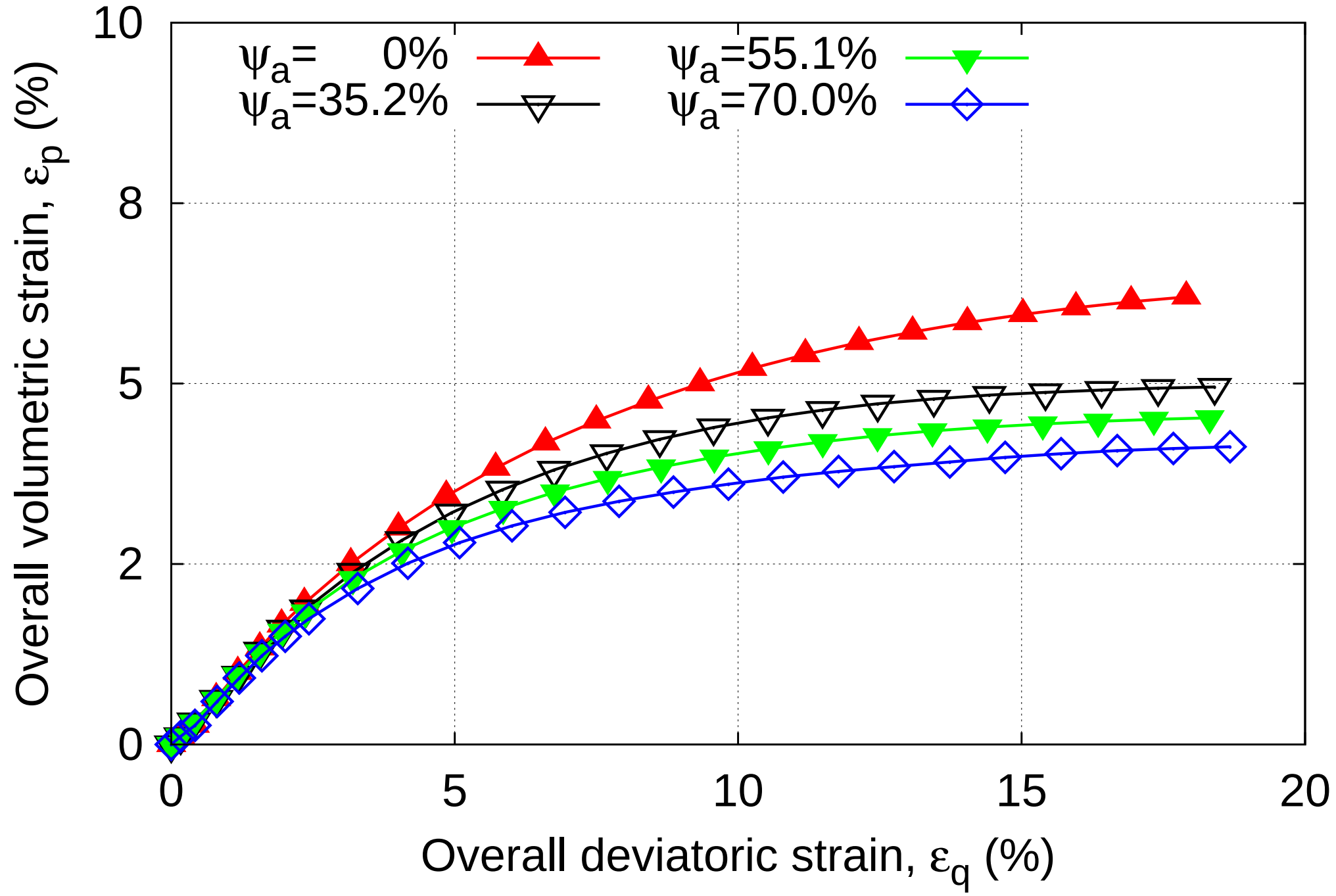

Figure 6b

Click here to access/download;Figure;Fig 6b.eps

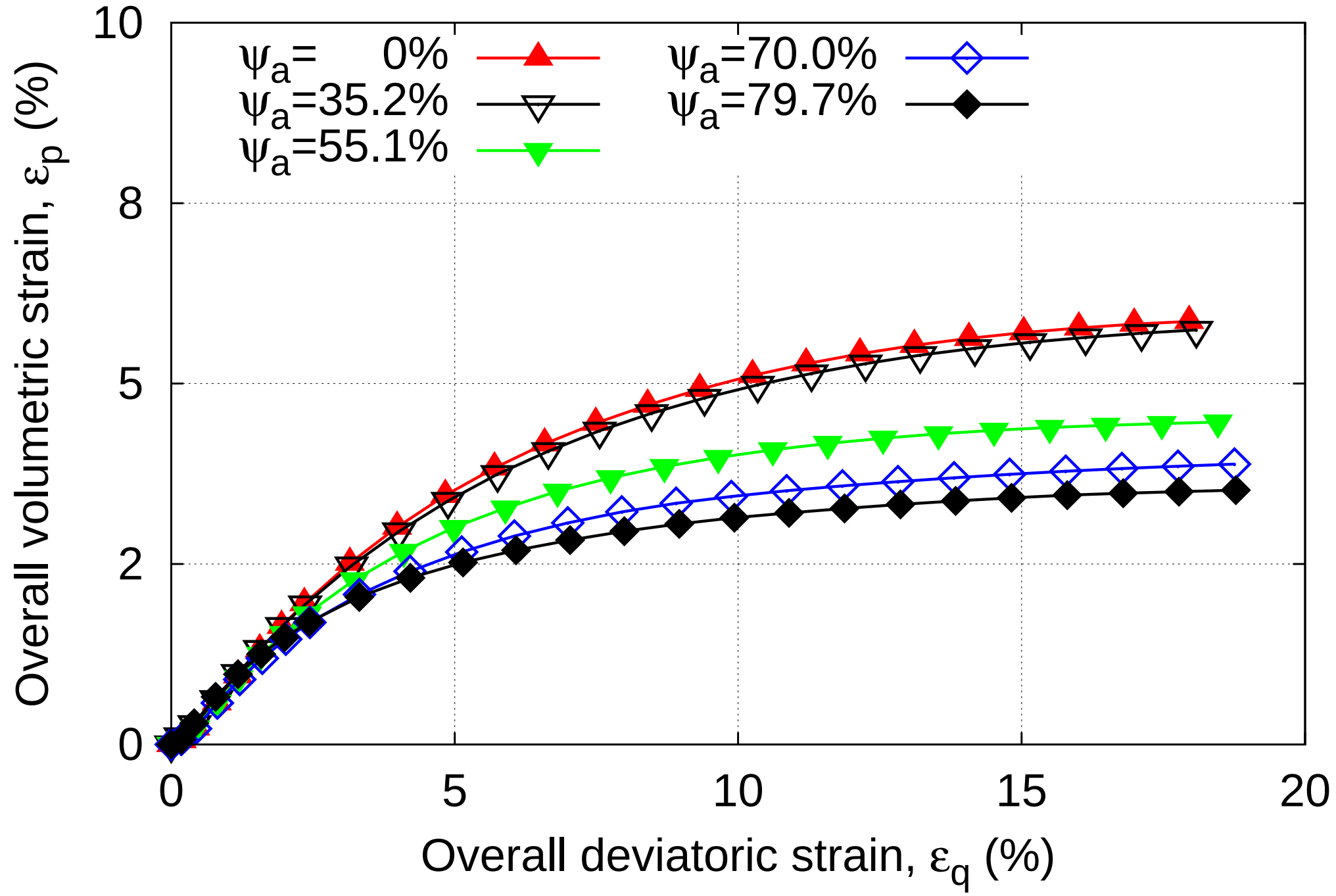

Figure 6c

Click here to access/download;Figure;Fig 6c.eps

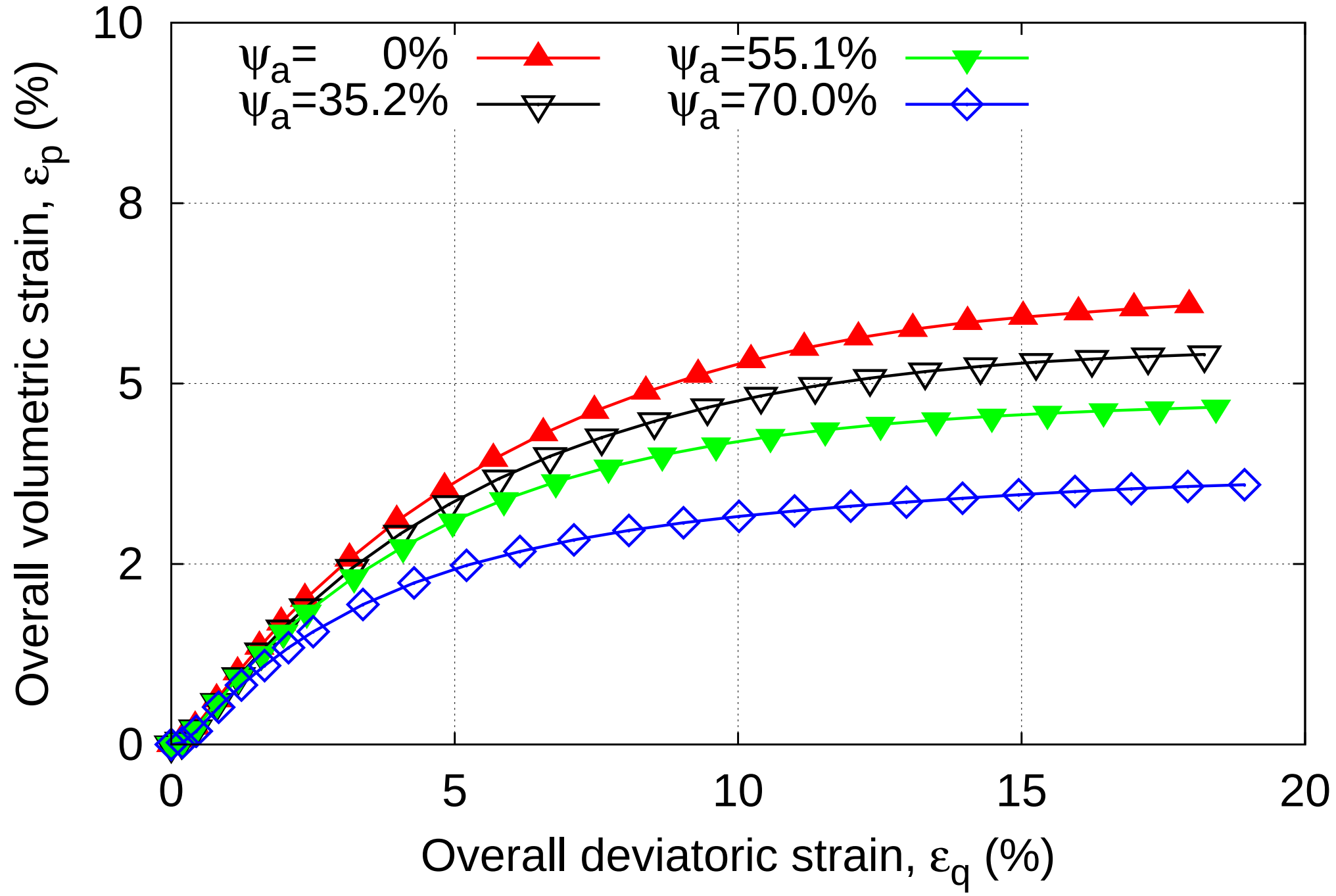

Figure 7a

Click here to access/download;Figure;Fig 7a.eps

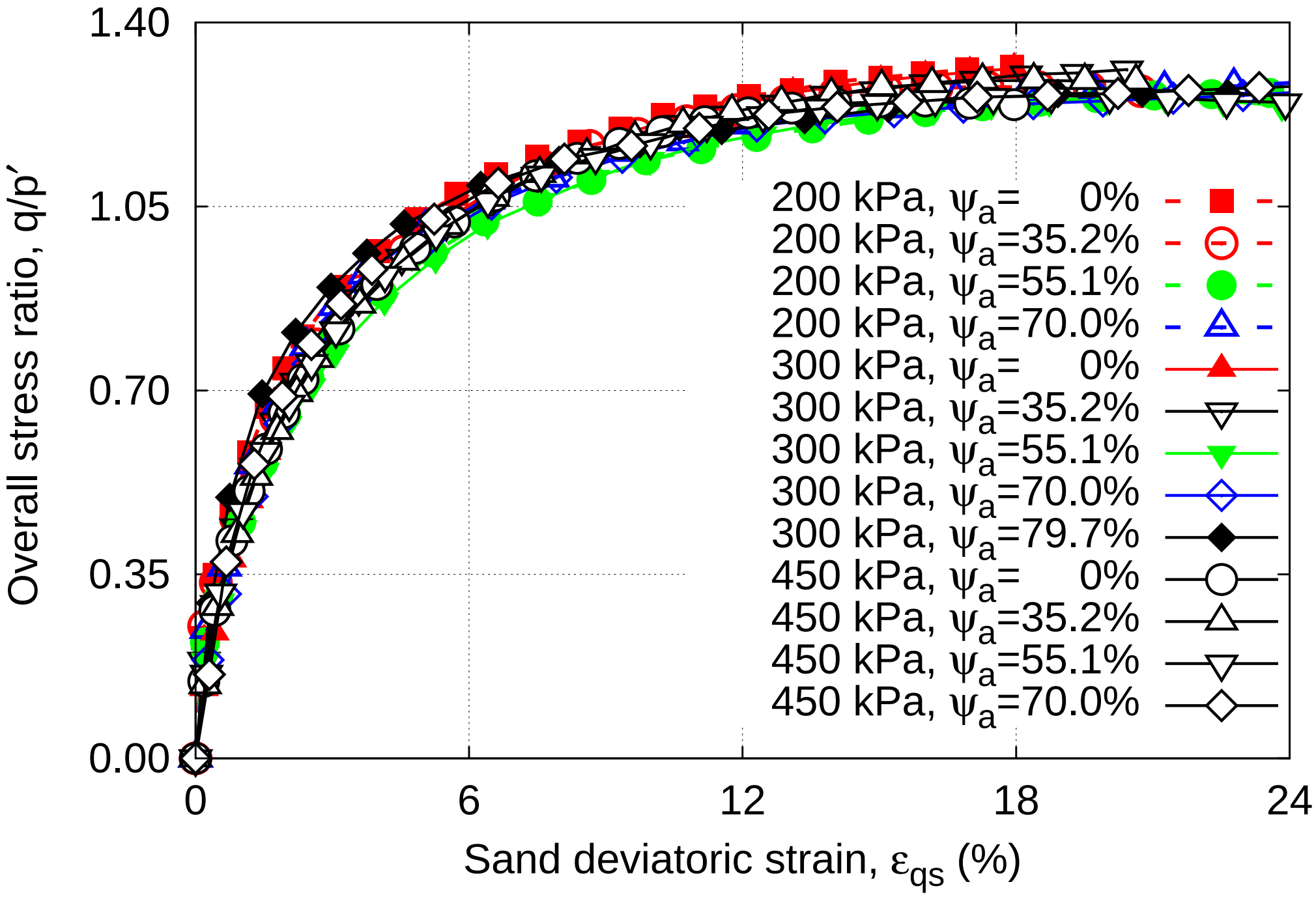

Figure 7b

Click here to access/download;Figure;Fig 7b.eps

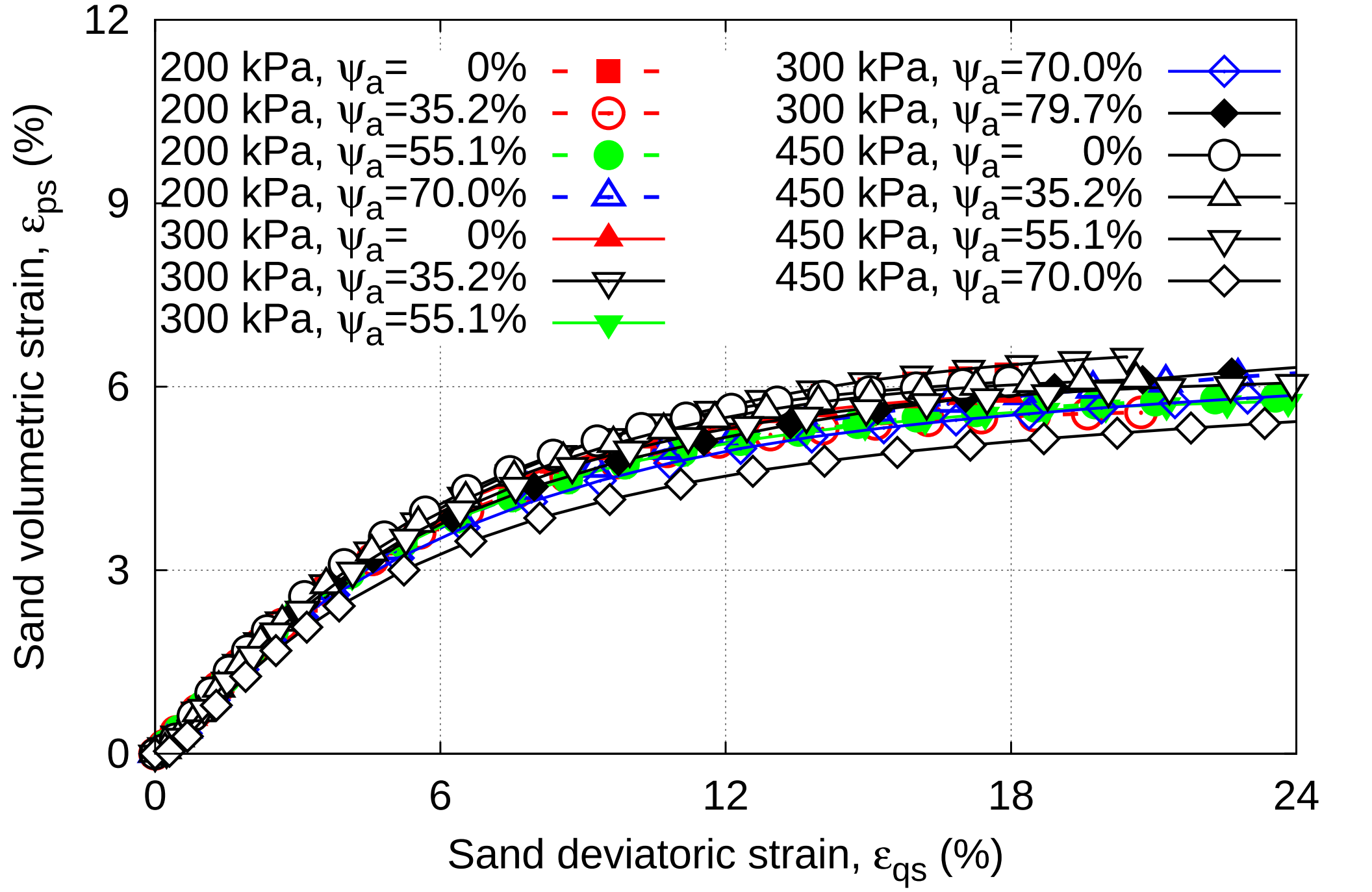

Figure 8a

Click here to access/download;Figure;Fig 8a.eps

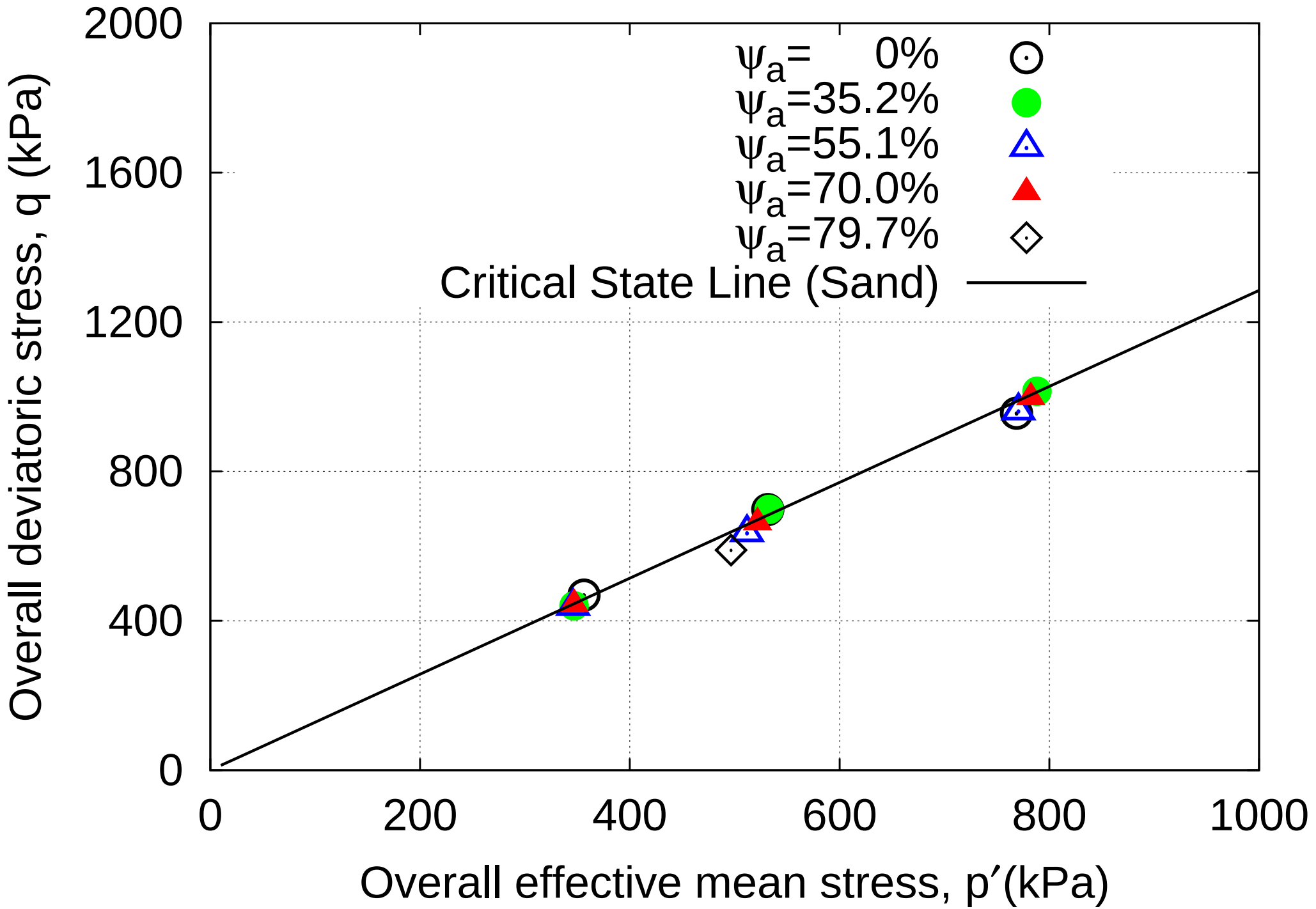

Figure 8b

Click here to access/download;Figure;Fig 8b.eps

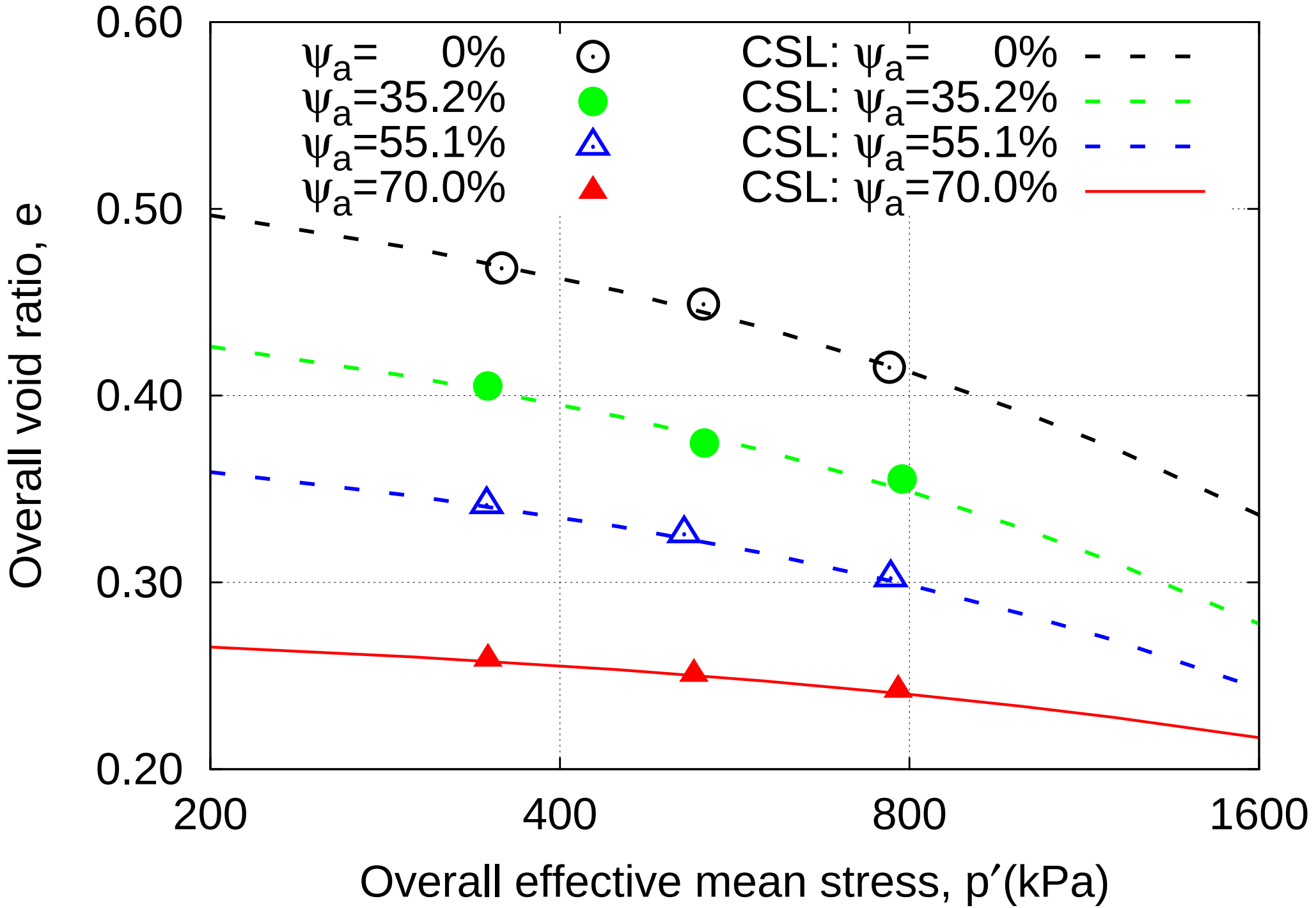

Figure 9a

Click here to access/download;Figure;Fig 9a.eps

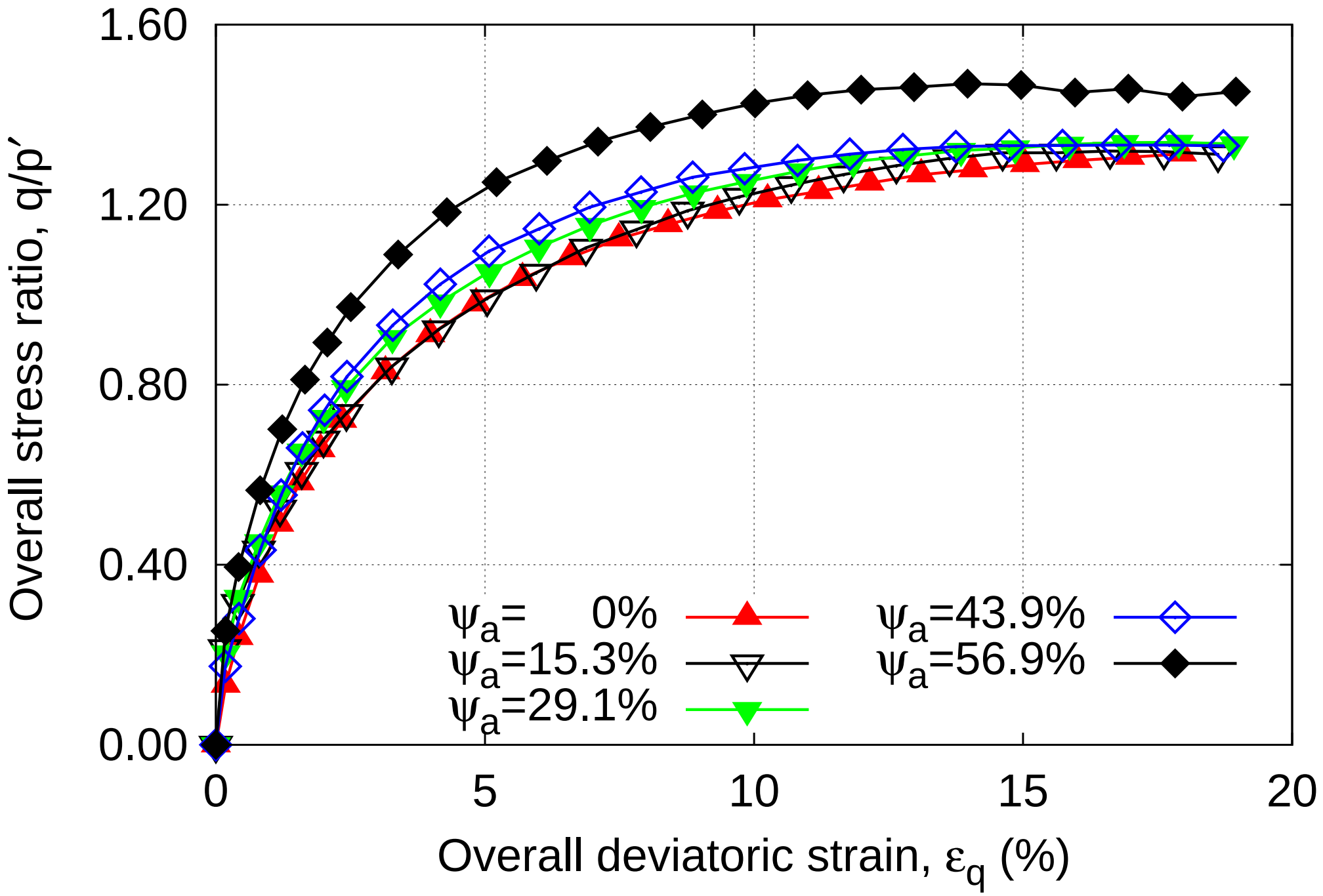

Figure 9b

Click here to access/download;Figure;Fig 9b.eps

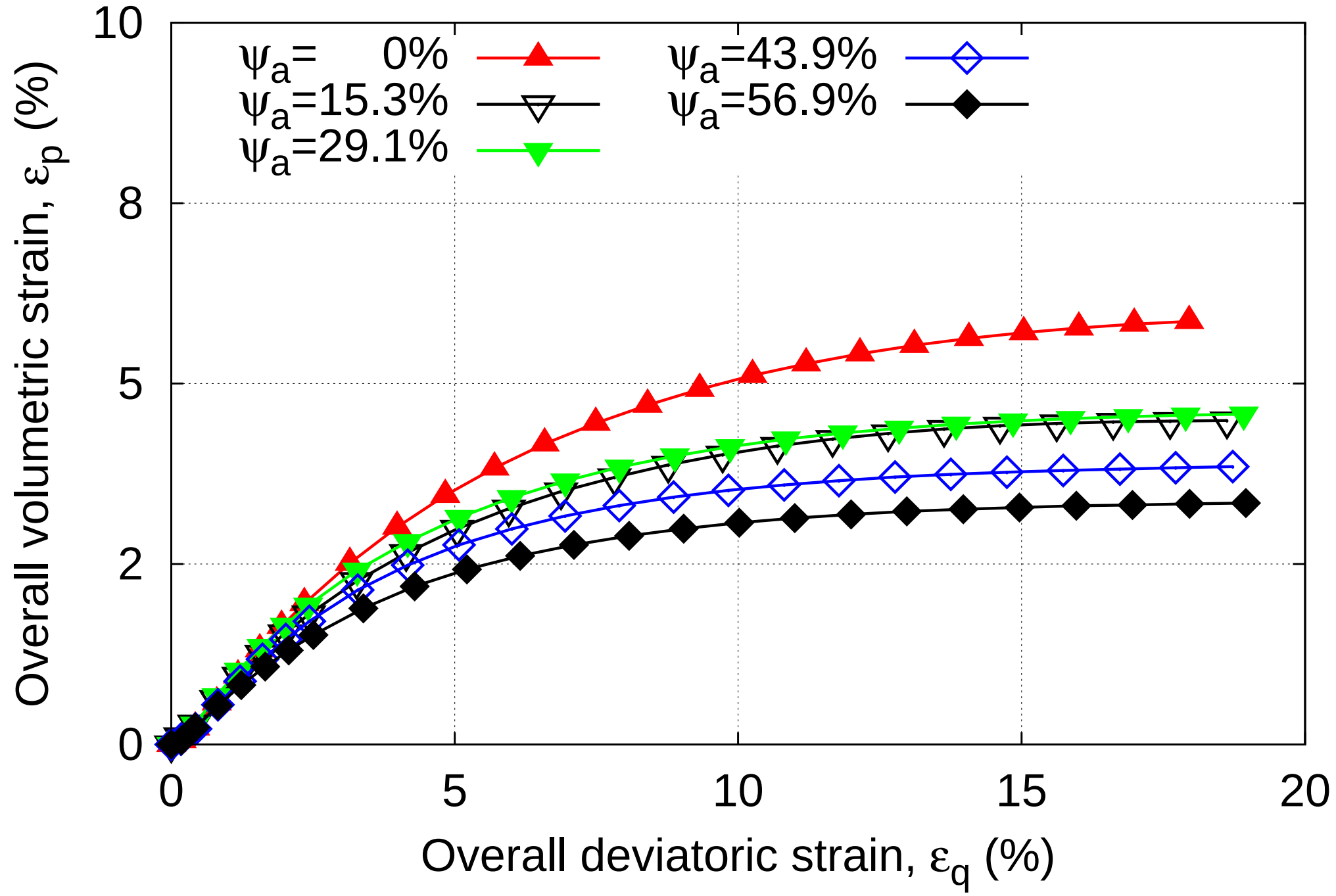

Figure 10a

Click here to access/download;Figure;Fig 10a.eps

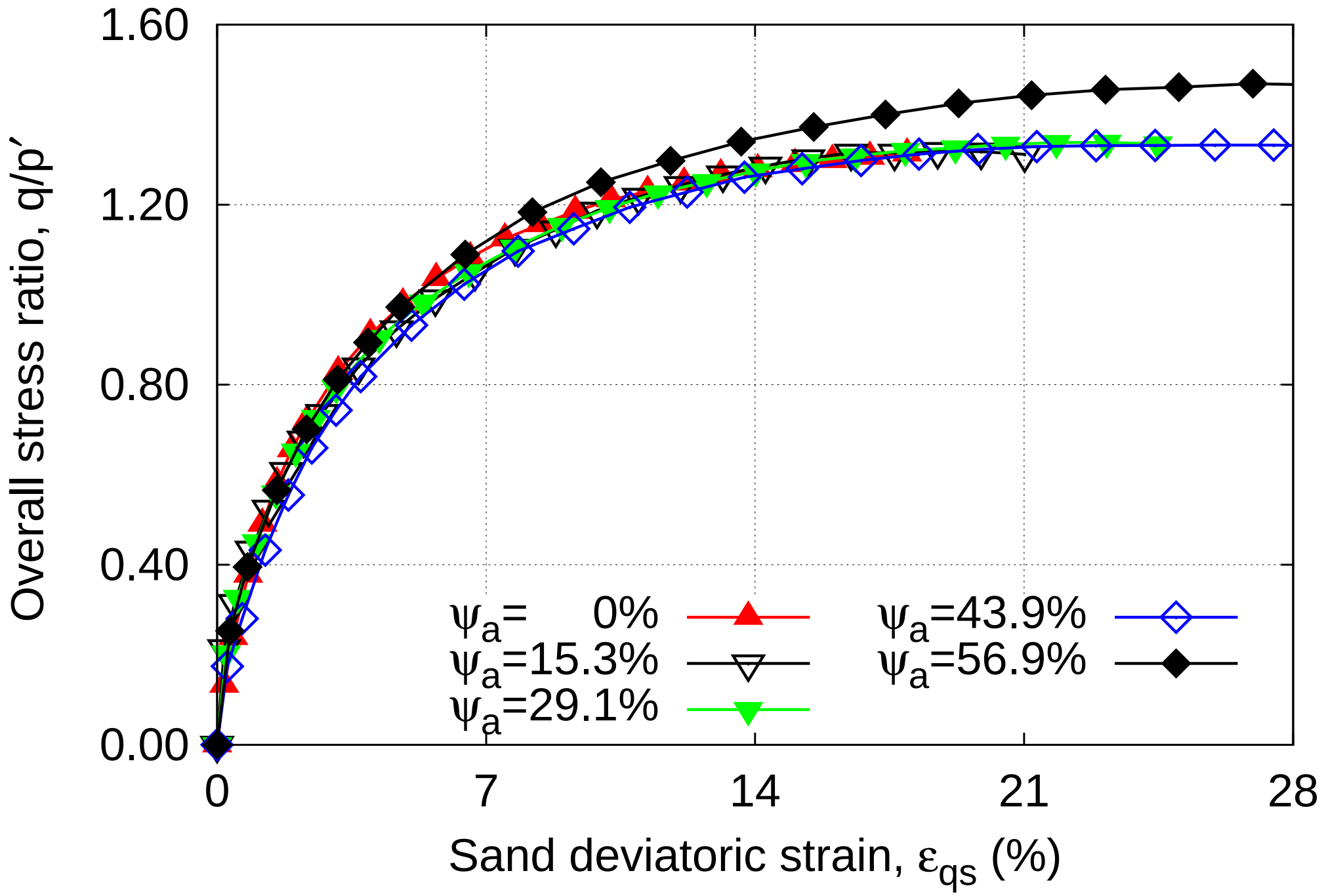

Figure 10b

Click here to access/download;Figure;Fig 10b.eps

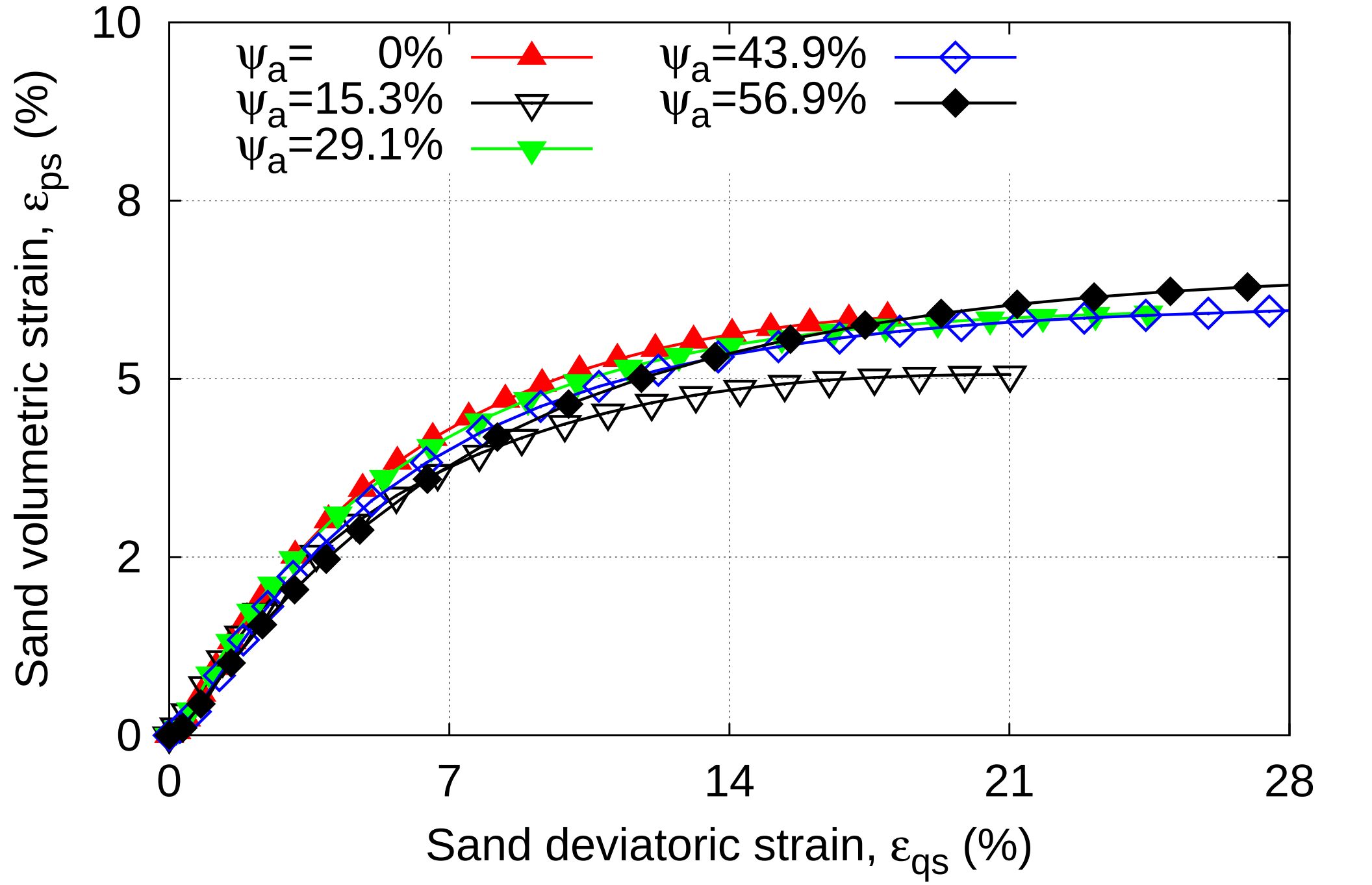

Figure 11a

Click here to access/download;Figure;Fig 11a.eps

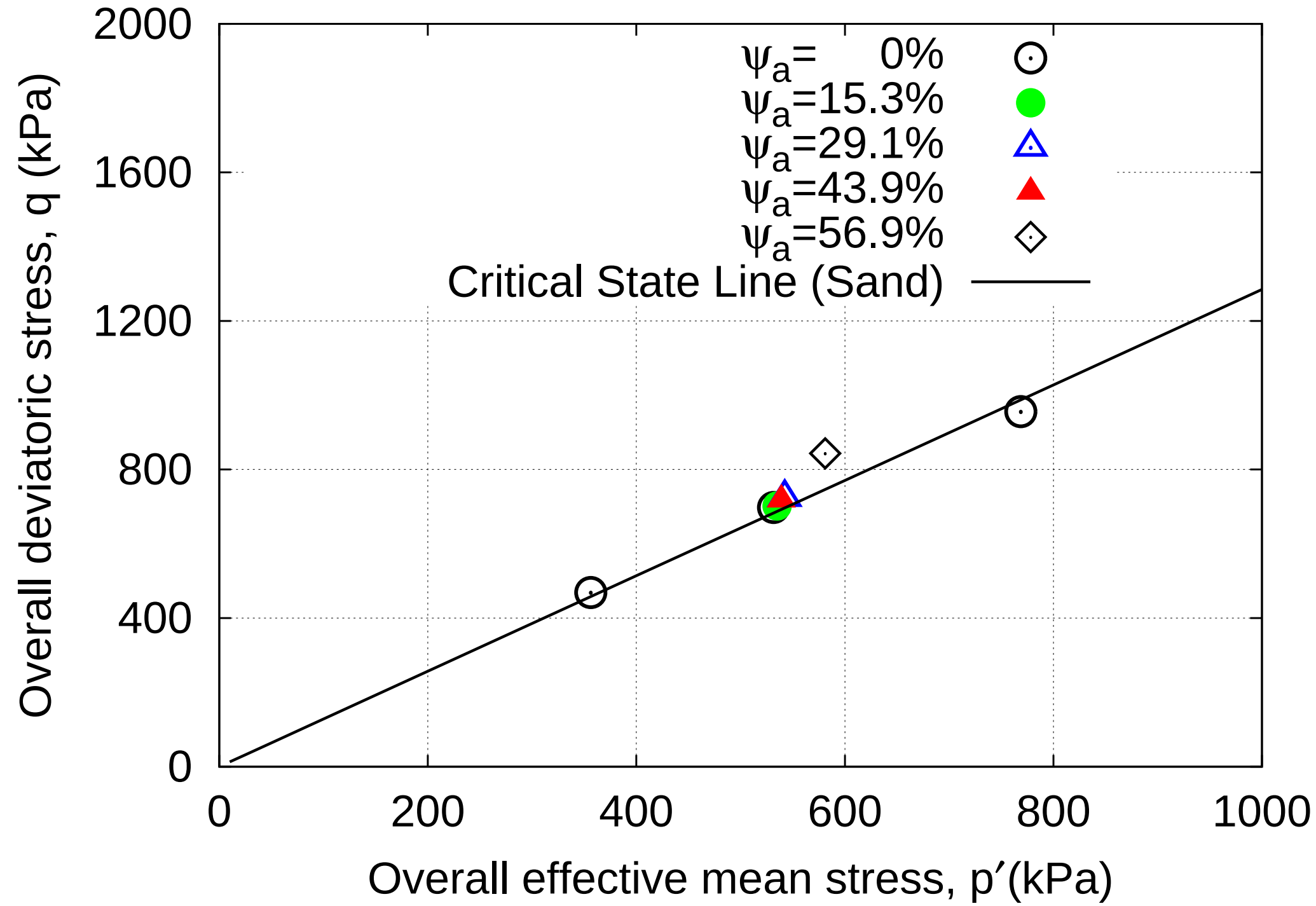

Figure 11b

Click here to access/download;Figure;Fig 11b.eps

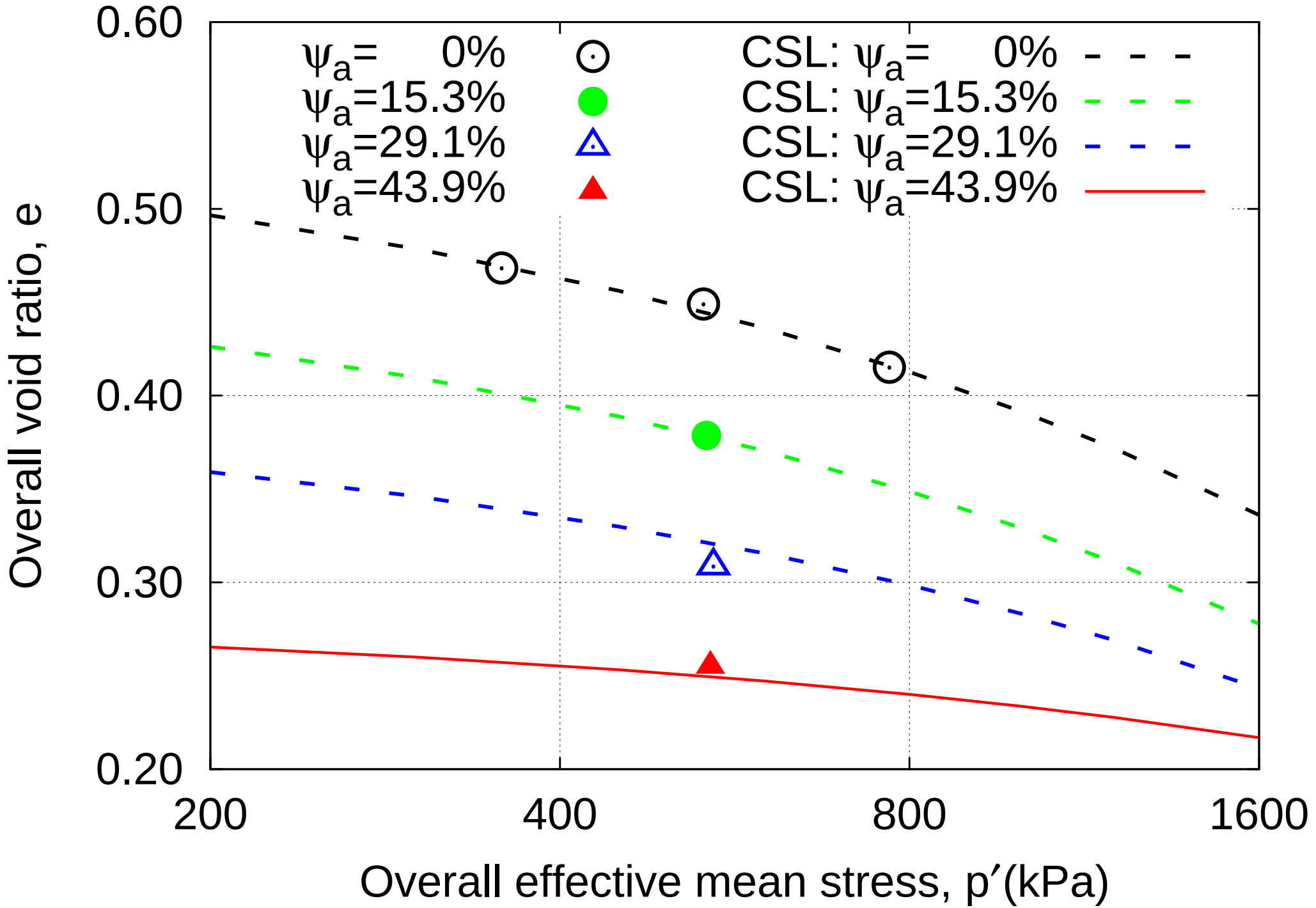

Figure 12a

Click here to access/download;Figure;Fig 12a.eps

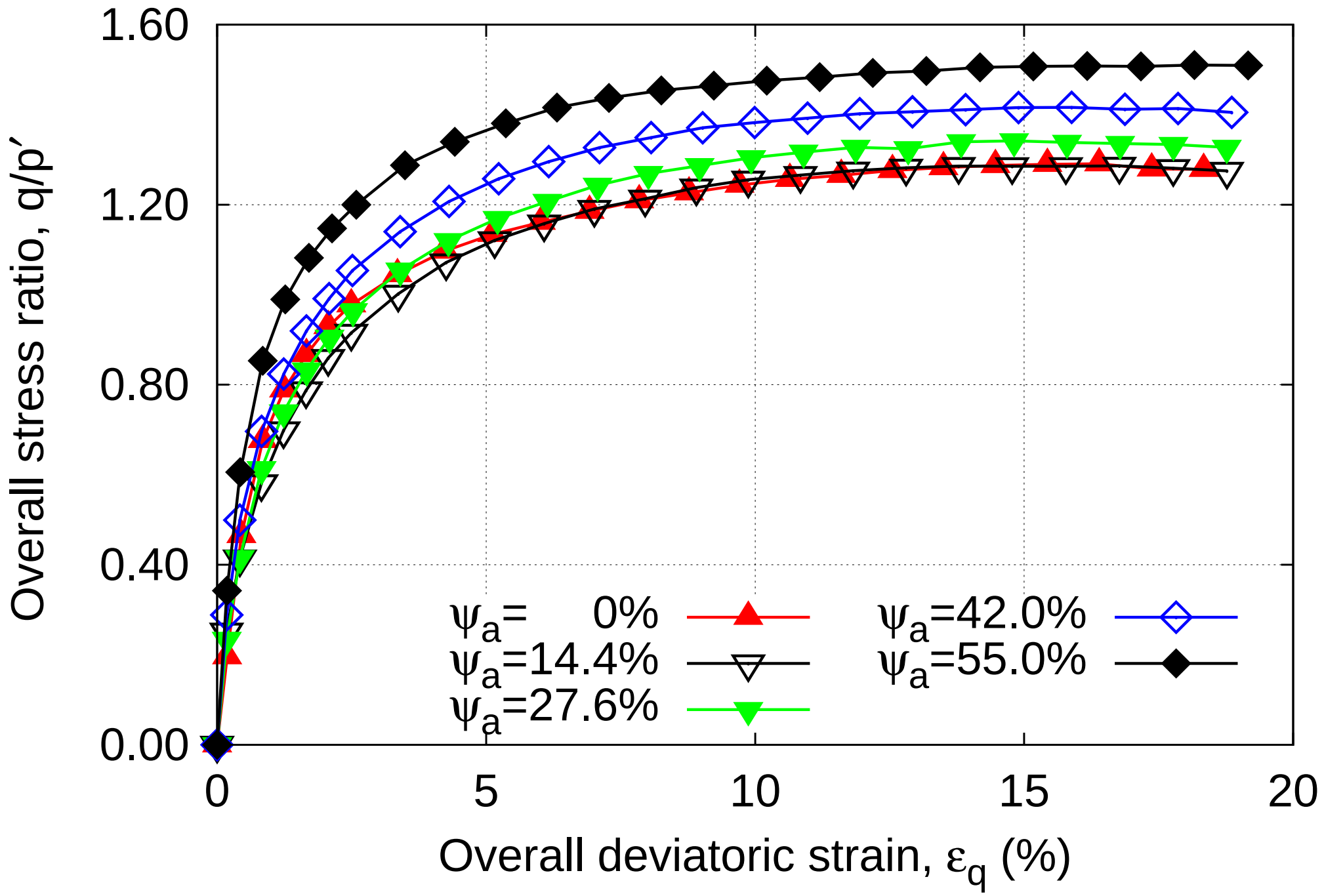

Figure 12b

Click here to access/download;Figure;Fig 12b.eps

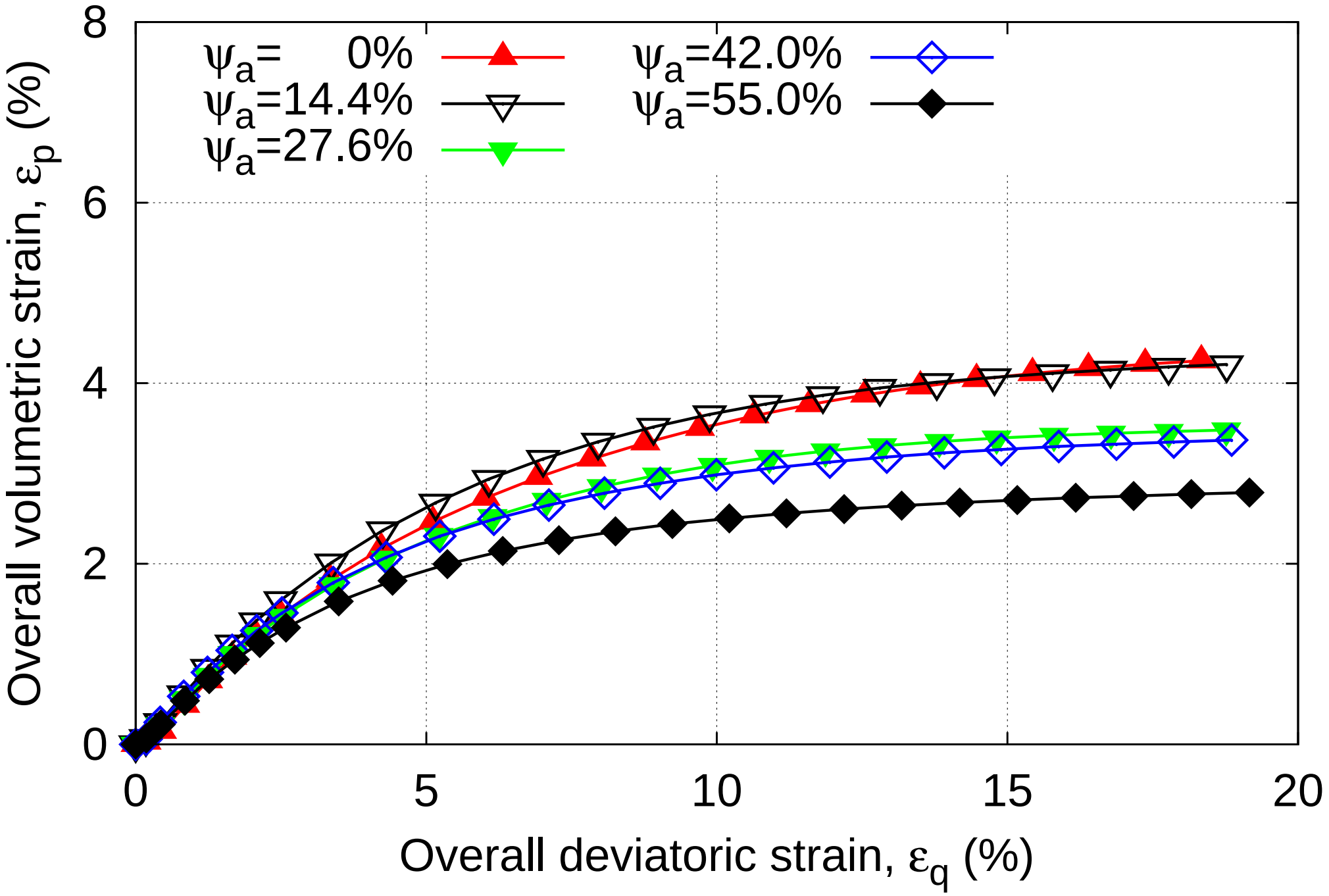

Figure 13a

Click here to access/download;Figure;Fig 13a.eps

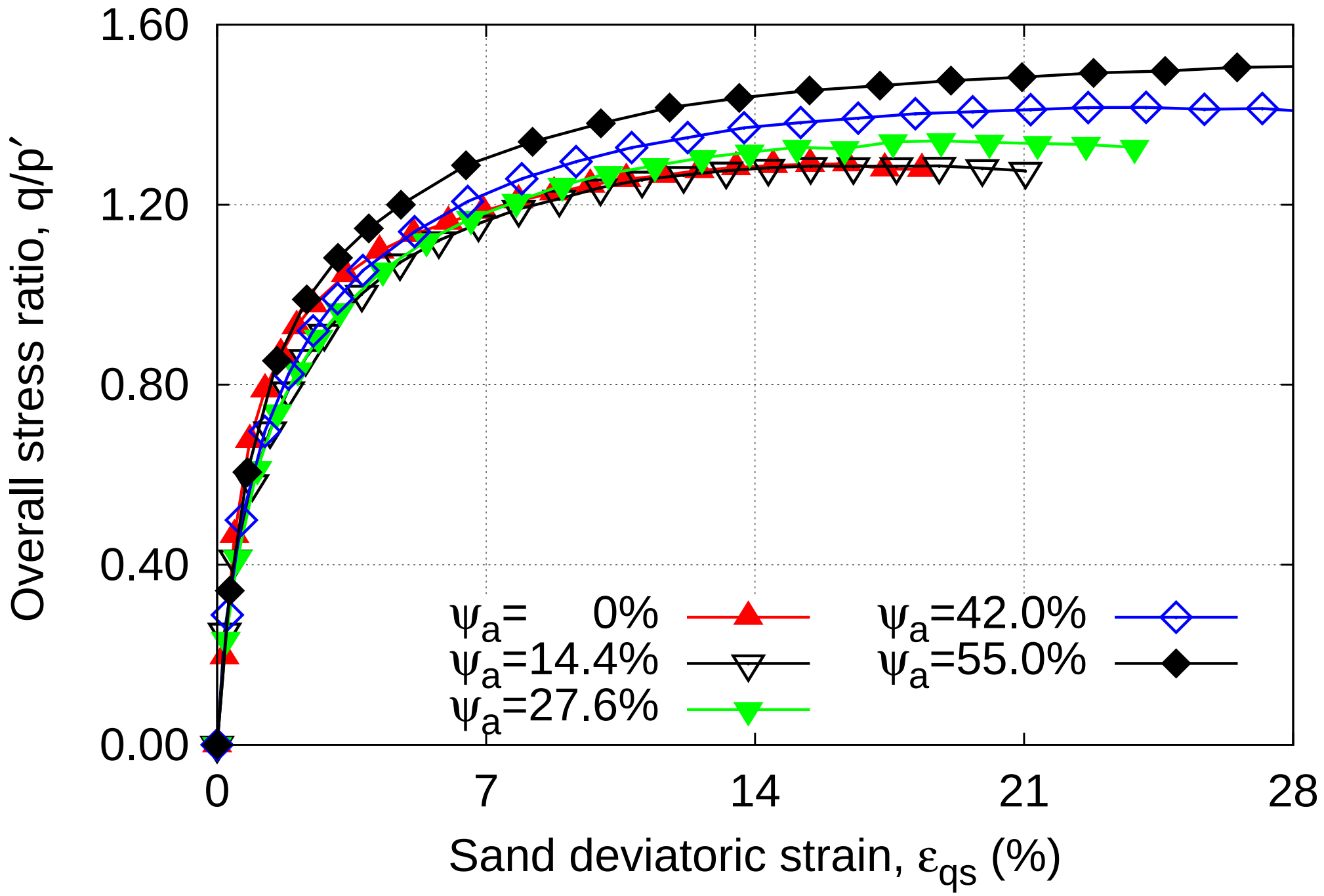

Figure 13b

Click here to access/download;Figure;Fig 13b.eps

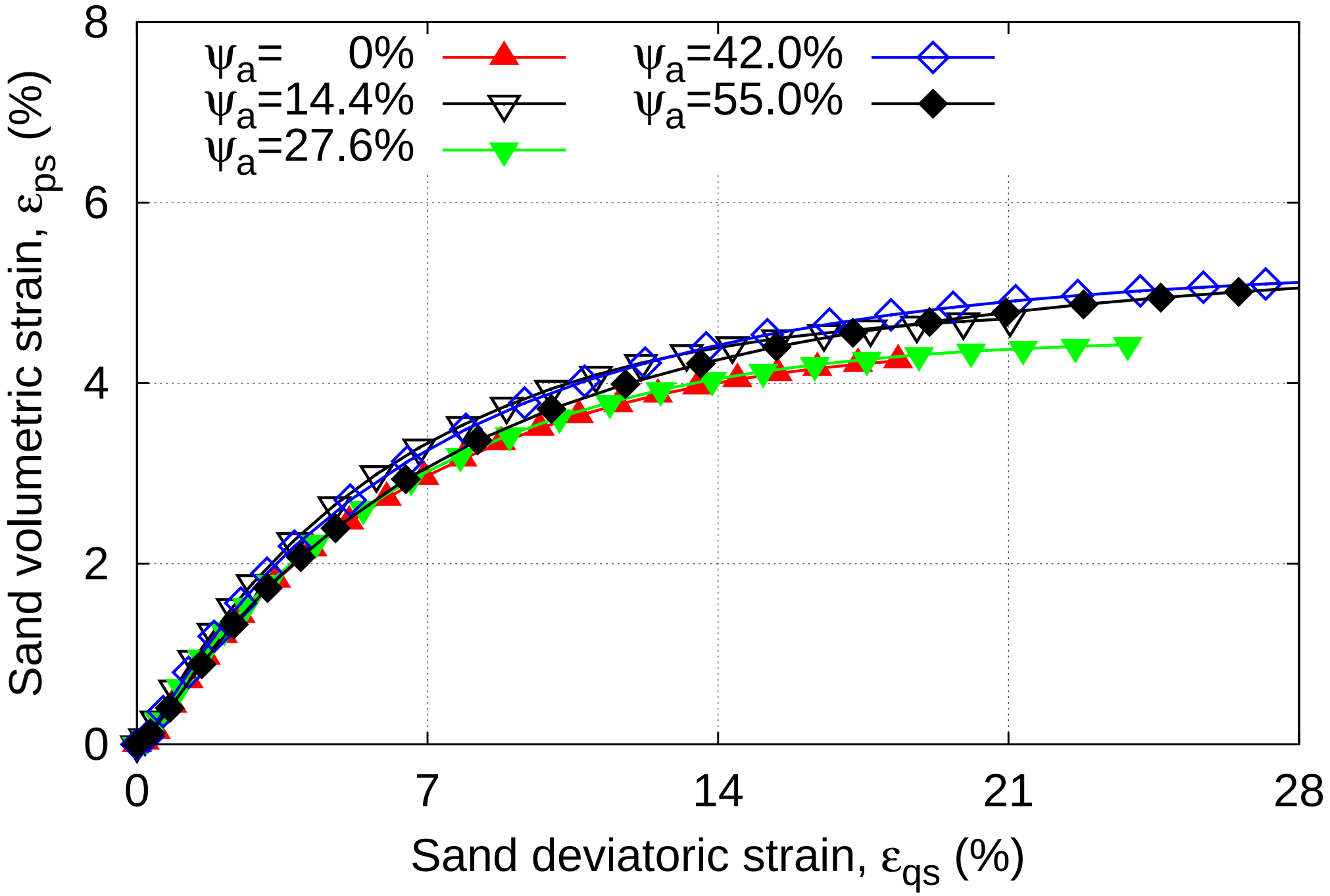

Figure 14a

Click here to access/download;Figure;Fig 14a.eps

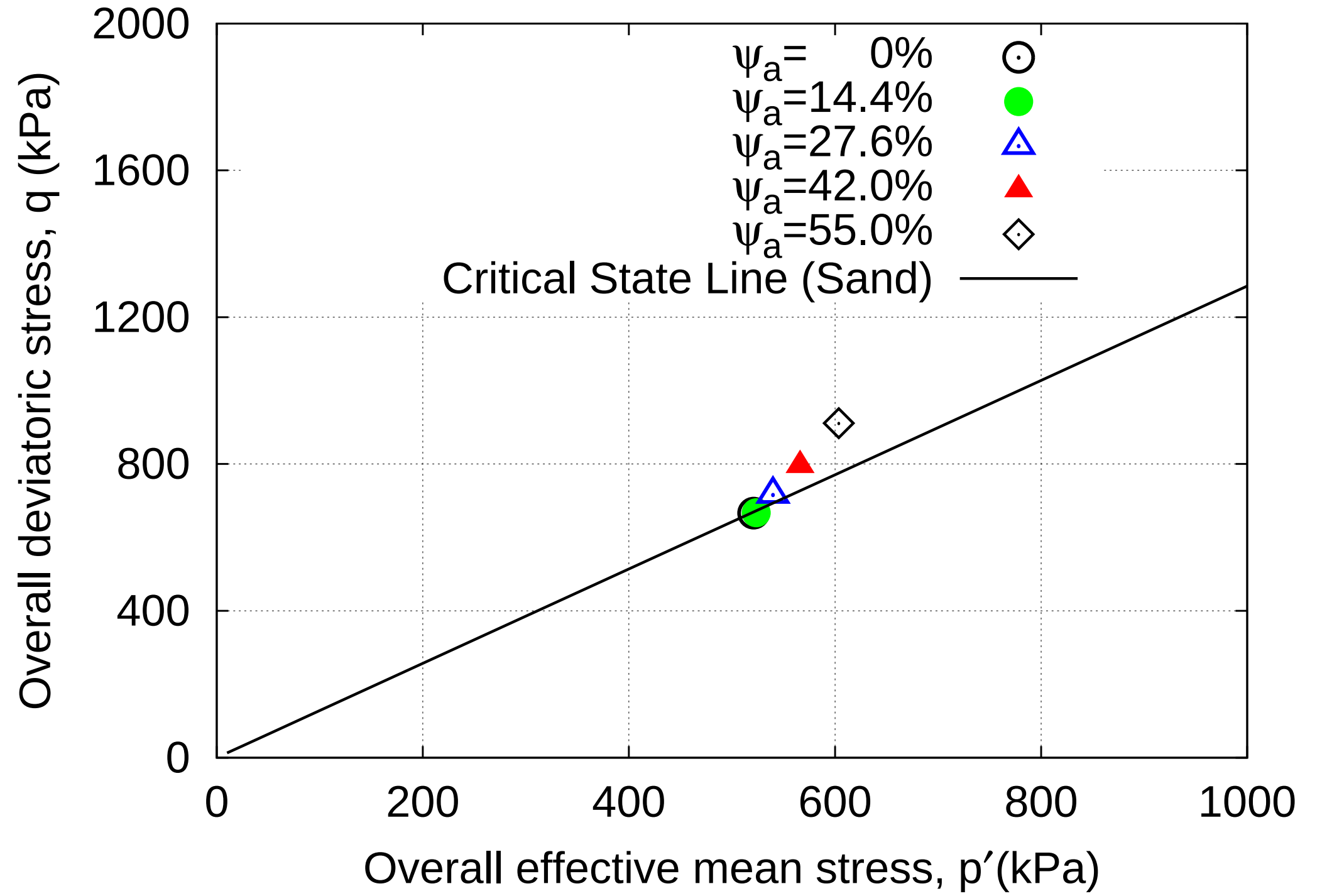

Figure 14b

Click here to access/download;Figure;Fig 14b.eps

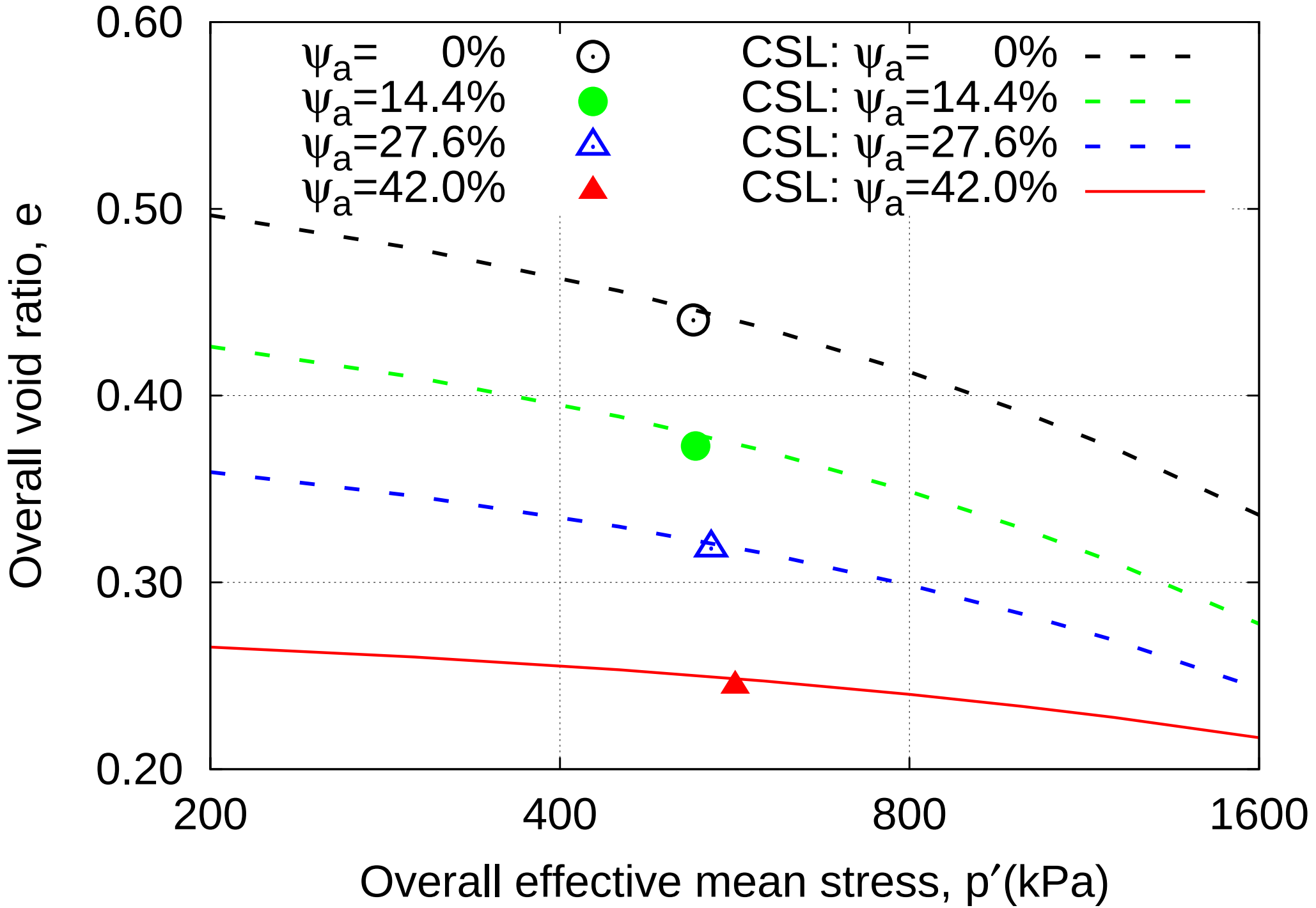

Figure 15

Click here to access/download;Figure;Fig 15.pdf

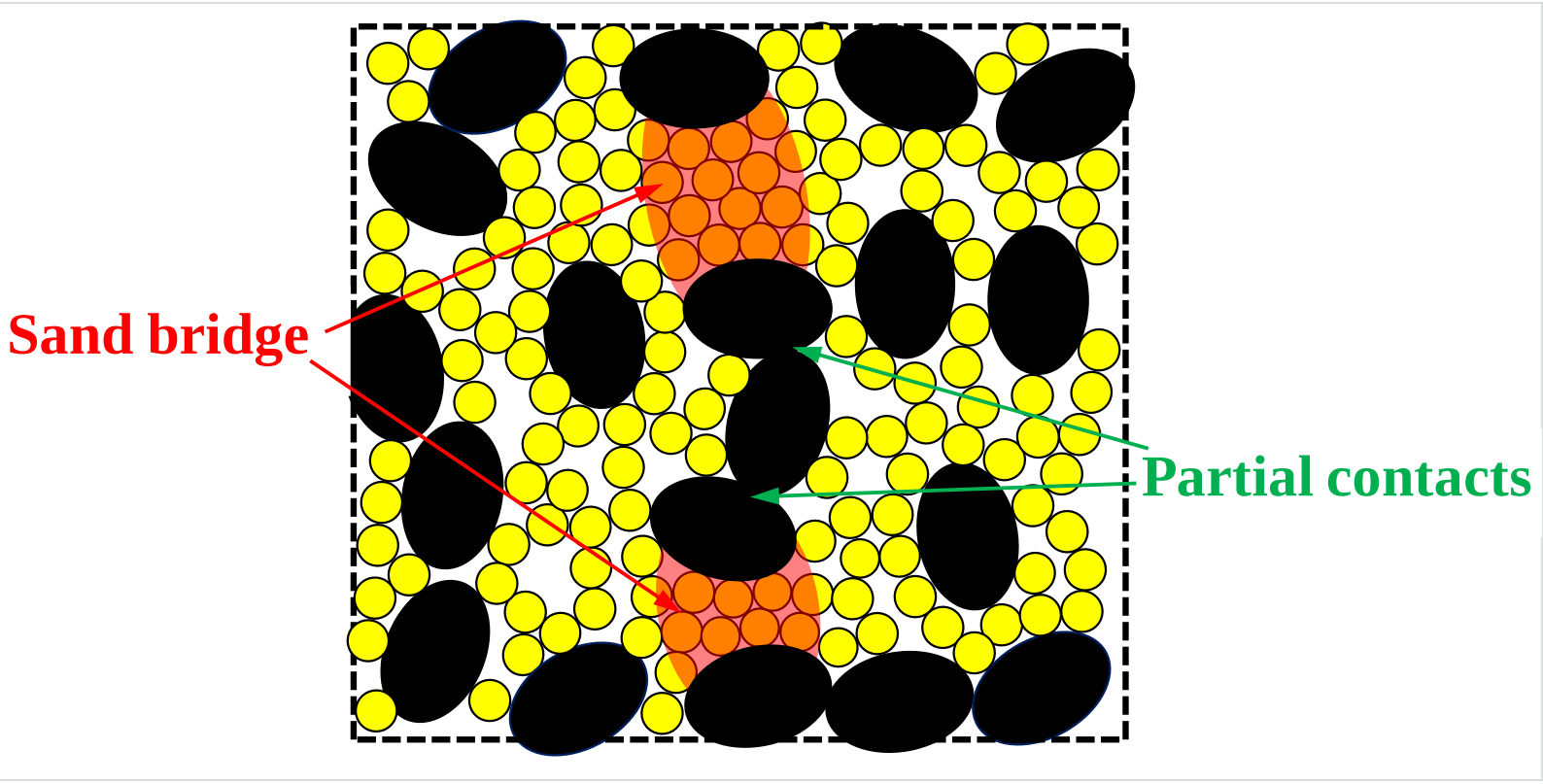

List of Figures

22 sand deviatoric strain ε_{qs} vs. stress ratio $\frac{q}{p'}$, (b) sand deviatoric strain ε_{qs} vs. sand

23 volumetric strain ε_{ps}

24 Figure 11. Critical state of gap-graded soils (loose sand + gravel) in drained triaxial

25 compression tests: (a) stress plane, (b) compression plane

26 Figure 12. Drained triaxial compression tests on gap-graded soils (dense sand + gravel): (a)

27 deviatoric strain ε_q and stress ratio $\frac{q}{p'}$, (b) deviatoric strain ε_q and volumetric strain ε_p

28 Figure 13. Drained triaxial compression tests on gap-graded soils (dense sand + gravel): (a)

29 sand deviatoric strain ε_{qs} vs. stress ratio $\frac{q}{p'}$, (b) sand deviatoric strain ε_{qs} vs. sand

30 volumetric strain ε_{ps}

31 Figure 14. Critical state of gap-graded soils (dense sand + gravel) in drained triaxial

32 compression tests: (a) stress plane, (b) compression plane

33 Figure 15. Partial contacts and sand bridges in gap-graded granular materials